

Phase transition from nuclear matter to color superconducting quark matter

W. Bentz *, T. Horikawa

Department of Physics, School of Science, Tokai University
Hiratsuka-shi, Kanagawa 259-1292, Japan

N. Ishii

The Institute of Physical and Chemical Research (RIKEN)
Hirosawa, Wako-shi, Saitama 351-0198, Japan

A.W. Thomas

Special Research Centre for the Subatomic Structure of Matter
and

Department of Physics and Mathematical Physics,
The University of Adelaide
Adelaide, SA 5005, Australia

*Correspondence to: W. Bentz, E-mail: bentz@keyaki.cc.u-tokai.ac.jp

Abstract

We construct the nuclear and quark matter equations of state at zero temperature in an effective quark theory (the Nambu-Jona-Lasinio model), and discuss the phase transition between them. The nuclear matter equation of state is based on the quark-diquark description of the single nucleon, while the quark matter equation of state includes the effects of scalar diquark condensation (color superconductivity). The effect of diquark condensation on the phase transition is discussed in detail.

PACS: 12.39.Fe, 12.39.Ki, 21.65.+1, 24.85+p, 64.70.Fx, 05.70.-a

Keywords: Equation of state, Effective quark theories, Diquark condensation, Phase transitions

1 Introduction

The behavior of matter at high baryon density is of great interest in connection with neutron stars, the possible existence of quark stars [1], and heavy ion collisions [2]. At normal densities, hadronic matter consists of three-quark (nucleon-like [3]) clusters, and the forces between them lead to the familiar saturation properties of nuclear matter (NM). At high densities one expects a phase transition to quark matter (QM) [4], but the dynamics of this transition, the transition densities, and the equation of state (EOS) in the high density regime are largely unknown. In many recent investigations it has been found that the QM state at high densities differs from a non-interacting quark gas. In particular, there is an instability with respect to diquark condensation, leading to a color superconducting state [5]-[7]. On the other hand, diquark correlations are known to play an important role in explaining the properties of single nucleons, for example the flavor dependence of the structure functions [8, 9]. At high baryon densities one therefore expects a phase transition from quark-diquark clusters to a diquark condensed phase.

Since it is still difficult to obtain unambiguous results for finite density matter directly from QCD, effective quark models provide powerful tools to investigate the behavior of matter as the baryon density increases. Naturally, these models should account for the properties of the free nucleon in terms of constituent quarks, as well as for the saturation properties of nuclear matter at normal densities. They should also allow for the possibility of a high density QM phase, where chiral symmetry is restored and color symmetry spontaneously broken. In these respects, the Nambu-Jona-Lasinio (NJL) model [10, 11] is an attractive candidate. First, the simplicity of the model

allows a direct solution of the relativistic Faddeev equation [12], leading to a covariant and successful description of the single nucleon [13]-[16]. Second, it has been shown recently [17] that this successful quark-diquark description of the single nucleon can be extended to describe the EOS of NM. The essential ingredient needed to obtain a saturating EOS was to simulate the effect of confinement by introducing an infrared cut-off (in addition to the usual ultraviolet one) in order to avoid unphysical thresholds corresponding to the decay of hadrons into free quarks [21]. Third, models of the NJL-type are able to describe a high density QM state where chiral symmetry is restored and color symmetry is broken [5]. It is, of course, desirable to combine these three aspects and describe nucleons, NM and superconducting QM in one consistent framework. This is the purpose of our present work.

In this paper we will investigate the role of diquark condensation for the phase transition from NM to QM in the NJL model. It is clear that diquark condensation will soften the EOS of QM and favor the phase transition. The transition densities are therefore expected to decrease with increasing pairing strength. We will investigate this relation, and discuss a possible scenario for the phase transition. In the course of the calculation we will face the problem of whether or not those parameters of the model which have been determined exclusively by the properties of single nucleons and NM, like the value of the infrared cut-off, the strength of the $q\bar{q}$ interaction in the vector meson channel, and the strength of the qq interaction in the scalar diquark channel, should be taken over to QM. In order to discuss these points, in particular the strength of the $q\bar{q}$ interaction in the vector meson channel, we will also consider the ω meson mass in the medium. Another purpose of this work is to present a consistent formulation which accounts

for the three aspects discussed above - i.e., the single nucleon, normal NM and superconducting QM.

In sect. 2 we will first explain the model in the framework of the Nambu-Gorkov formalism [22, 23], and then use path integral methods to describe the single nucleon as well as the EOS for NM and QM. In sect. 3 we will present numerical results, and discuss the role of diquark condensation in the phase transition. Finally, we summarize our results in sect. 4.

2 NJL model in the Nambu-Gorkov formalism

The Lagrangian density of the flavor SU(2) NJL model has the general form $\mathcal{L} = \bar{\psi} (i\not{\partial} - m) \psi + \sum_{\alpha} G_{\alpha} (\bar{\psi} \Gamma_{\alpha} \psi)^2$, where m is the current quark mass, and the chirally symmetric 4-fermi interaction is characterized by the matrices Γ_{α} in Dirac, flavor and color space, and the corresponding coupling constants G_{α} . Hadronization techniques to describe the single nucleon and NM, as well as the description of superconducting QM, are simplified very much if one makes use of the Nambu-Gorkov formalism [22, 23]. In this method, the Lagrangian density is re-written identically in terms of the fields ¹

$$\Psi = \frac{1}{\sqrt{2}} \begin{pmatrix} \psi \\ C\tau_2\bar{\psi}^T \end{pmatrix}, \quad \bar{\Psi} = \frac{1}{\sqrt{2}} (\bar{\psi}, -\psi^T\tau_2C^{-1}), \quad (2.1)$$

where $C = i\gamma_0\gamma_2$, as follows:

$$\mathcal{L} = \bar{\Psi} (i\not{\partial} - m) \Psi + \sum_{\alpha M} G_{\alpha} (\bar{\Psi} \Gamma_{\alpha} \sigma_M \Psi)^2. \quad (2.2)$$

¹Since there is freedom under unitary transformations to define the field Ψ , the presence of the matrices C and τ_2 in the lower components is a matter of definition. We include them here because they lead to simplifications in some of the following formulae.

We denote the matrices in the Nambu-Gorkov space by $\sigma_M \equiv (\sigma_0, \sigma_3)$ for the interactions in mesonic ($q\bar{q}$) channels, and by $\sigma_D \equiv (\sigma_1, \sigma_2)$ for the diquark (qq) channels. Here σ_0 is the 2×2 unit matrix, and $\sigma_1, \sigma_2, \sigma_3$ are the usual Pauli matrices. It is easy to verify that the only non-zero terms in (2.2) are those which satisfy

$$C \tau_2 \sigma_2 \Lambda_\alpha^T C^{-1} \sigma_2 \tau_2 = \Lambda_\alpha, \quad (2.3)$$

where $\Lambda_\alpha \equiv \Gamma_\alpha \sigma_M$. Therefore, for a given Γ_α , either $M = 0$ or $M = 3$ contributes in (2.2).

Any Lagrangian density of the form (2.2) can further be re-written into a Fierz symmetric form [12], where the interactions in the diquark channels, characterized by σ_D , also appear. For these terms to be non-zero, the same condition (2.3) holds with $\Lambda_\alpha \equiv \Gamma_\alpha \sigma_D$. The coupling constants appearing in the Fierz symmetric Lagrangian density for the various meson and diquark channels are linear combinations of the G_α 's appearing in the Lagrangian density (2.2). For the purposes of this work, we will need only the following terms:

$$\begin{aligned} \mathcal{L}_I &= G_\pi \left((\bar{\Psi}\Psi)^2 + (\bar{\Psi} i \gamma_5 \boldsymbol{\tau} \sigma_3 \Psi)^2 \right) \\ &- G_\omega (\bar{\Psi} \gamma^\mu \sigma_3 \Psi)^2 + G_s (\bar{\Psi} i \gamma_5 \sigma_D \beta_a \Psi)^2, \end{aligned} \quad (2.4)$$

which are the interactions in the $(J^P, T) = (0^+, 0), (0^-, 1)$ and $(1^-, 0)$ color singlet meson channels, and the $(0^+, 0)$ color $\bar{3}$ diquark (scalar diquark) channel. The color $\bar{3}$ matrices are defined in terms of the antisymmetric Gell-Mann matrices by $\beta_a = \sqrt{3/2} \lambda_A$, where $a = 1, 2, 3$ corresponds to $A = 2, 5, 7$. A sum over $D = 1, 2$ and $a = 1, 2, 3$ is implied in the last term of Eq.(2.4).

The 3 coupling constants in Eq.(2.4) will be treated as free parameters.

The values of the ratios

$$r_s \equiv \frac{G_s}{G_\pi}, \quad r_\omega \equiv \frac{G_\omega}{G_\pi} \quad (2.5)$$

reflect the form of the original interaction Lagrangian density (2.2).

The 4-fermi interactions, $G_\alpha (\bar{\Psi} \Lambda_\alpha \Psi)^2$, in Eq.(2.4) can be eliminated in favor of bosonic auxiliary fields b_α as usual² by subtracting terms of the form $(2G_\alpha \bar{\Psi} \Lambda_\alpha \Psi + b_\alpha)^2 / 4G_\alpha$, which are formally equal to zero if we impose the constraints (equations of motion) $\partial \mathcal{L} / \partial b_\alpha = 0$. In this way we obtain the partially bosonized Lagrangian density in the form:

$$\begin{aligned} \mathcal{L} = & \bar{\Psi} (i\not{\partial} - m - \Sigma - i\gamma_5 \boldsymbol{\tau} \cdot \boldsymbol{\pi} \sigma_3 - \not{\phi} \sigma_3 - i\gamma_5 \sigma_D \Delta_{Da} \beta_a) \Psi \\ & - \frac{1}{4G_\pi} (\Sigma^2 + \boldsymbol{\pi}^2) + \frac{1}{4G_\omega} \omega_\mu^2 - \frac{1}{4G_s} \Delta_{Da}^2, \end{aligned} \quad (2.6)$$

where the real bosonic auxiliary fields are defined by

$$\Sigma = -2G_\pi \bar{\Psi} \Psi; \quad \boldsymbol{\pi} = -2G_\pi \bar{\Psi} i \gamma_5 \boldsymbol{\tau} \sigma_3 \Psi, \quad (2.7)$$

$$\omega^\mu = 2G_\omega \bar{\Psi} \gamma^\mu \sigma_3 \Psi; \quad \Delta_{Da} = -2G_s \bar{\Psi} i \gamma_5 \beta_a \sigma_D \Psi. \quad (2.8)$$

In the two terms of (2.6) involving the diquark fields, a sum over $D = 1, 2$ and $a = 1, 2, 3$ is implied.

3 Nucleons, nuclear matter, and color superconducting quark matter

In this section we will use the Lagrangian density (2.6) to construct the single nucleon as a quark-scalar diquark state. We then use it to obtain the EOS of both NM and QM in the Hartree approximation.

²This procedure can also be formulated in the path integral formalism, as will be done in sect. 3 for the nucleon auxiliary field - see Eq.(3.9).

3.1 Nucleons and nuclear matter

The EOS of NM, based on the quark-diquark description of the single nucleon, has been derived in Ref.[17] by using a hybrid model to evaluate the expectation value of the quark Hamiltonian in the NM ground state, similar in spirit to the model of Guichon and collaborators [3, 24]. Since it is one of the aims of this paper to present a consistent formulation of the single nucleon, NM and QM in one framework, we will follow the path integral formalism based on the quark Lagrangian density (2.6).

The general method to obtain the NM EOS is as follows: One first uses hadronization methods [25, 14] to derive an effective hadronic Lagrangian density of the σ -model type from the quark Lagrangian density, and introduces a chemical potential for the nucleons. Then one can use any of the familiar approximation schemes for relativistic many-nucleon systems [26, 27]. In this paper we will limit ourselves to the Hartree approximation. For this purpose it is sufficient to derive the nucleon kinetic energy term in the presence of the mean meson fields, the c-number terms associated with the mean fields, and the “trace-log term” which emerges from the integration over the quark fields. Therefore, although the method outlined below can be used to obtain more complete expressions for the effective hadronic Lagrangian density, we will concentrate here on the nucleon kinetic energy term in the presence of mean scalar and vector fields.

We introduce the (color singlet) nucleon fields and sources by adding the following terms to the Lagrangian density (2.6):

$$\left[\bar{\mathcal{N}} + \frac{1}{\sqrt{3}} \bar{\Psi}_a \begin{pmatrix} \Delta_a^* & 0 \\ 0 & \Delta_a \end{pmatrix} \right] \Phi + \bar{\Phi} \left[\mathcal{N} + \frac{1}{\sqrt{3}} \begin{pmatrix} \Delta_a & 0 \\ 0 & \Delta_a^* \end{pmatrix} \Psi_a \right]. \quad (3.9)$$

Here the complex diquark fields are defined by $\Delta_a = \Delta_{1a} - i\Delta_{2a}$ and $\Delta_a^* =$

$\Delta_{1a} + i\Delta_{2a}$, and the Nambu-Gorkov fields, \mathcal{N} and Φ , are expressed in terms of the nucleon field, N , and the nucleon source, ϕ , in a similar manner to (2.1) for the quark fields. In the generating functional, the integrations over Φ and $\bar{\Phi}$ give functional δ -functions which show that the nucleon auxiliary fields must satisfy the constraints $N = -\psi_a \Delta_a / \sqrt{3}$ and $\bar{N} = -\bar{\psi}_a \Delta_a^* / \sqrt{3}$. The integrations over the nucleon fields then give unity – i.e., the terms (3.9) do not change the generating functional of the theory.

After integration over the quark fields (see Appendix A) we obtain the effective action ³

$$\mathcal{S}_{\text{eff}} = -\frac{i}{2} \text{Tr} \ln S^{-1} + \int d^4x \left(-\frac{\Delta_a^* \Delta_a}{4G_s} - \frac{(\Sigma^2 + \boldsymbol{\pi}^2)}{4G_\pi} + \frac{\omega_\mu^2}{4G_\omega} \right) \quad (3.10)$$

$$+ \frac{1}{3} \bar{\Phi} \begin{pmatrix} \Delta & 0 \\ 0 & \Delta^* \end{pmatrix} S \begin{pmatrix} \Delta^* & 0 \\ 0 & \Delta \end{pmatrix} \Phi + (\bar{\mathcal{N}}\Phi + \bar{\Phi}\mathcal{N}) \quad (3.11)$$

Here

$$S^{-1} = i\not{\partial} - m - \Sigma - i\gamma_5 \boldsymbol{\tau} \cdot \boldsymbol{\pi} \sigma_3 - \not{\omega} \sigma_3 - i\gamma_5 \begin{pmatrix} 0 & \Delta_a \beta_a \\ \Delta_a^* \beta_a & 0 \end{pmatrix}, \quad (3.12)$$

and S in (3.11) is the inverse of this. The meson and diquark fields are now the dynamical variables, while the nucleon field is still an auxiliary variable.

In NM the scalar and vector meson fields have non-zero expectation values, and accordingly one shifts the meson fields to separate these c-number parts from the fluctuation parts over which one has to integrate. Since we will describe the nucleon as a quark-diquark state (omitting mesonic fluctuations for the present), and the NM EOS in the Hartree approximation, we omit

³In the action, the symbol Tr includes also a functional trace. In order to avoid too many symbols, fields (propagators) will be frequently considered as vectors (matrices) in function space, besides their structures in color, flavor, and Dirac space. The notation \mathcal{S}_{eff} will be used generically for the effective action, irrespective of the space of fields where it operates.

the fluctuation parts of the bosonic fields from now, except for the scalar diquark field which will be used to construct the nucleon. That is, from now Σ and ω^μ will denote only the classical parts of the scalar and vector fields, which are expressed in terms of the quark fields $\psi, \bar{\psi}$ as ⁴

$$\Sigma \equiv -2G_\pi \langle \text{NM} | \bar{\psi} \psi | \text{NM} \rangle \equiv M - m, \quad \omega^\mu \equiv 2G_\omega \langle \text{NM} | \bar{\psi} \gamma^\mu \psi | \text{NM} \rangle \quad (3.13)$$

where $|\text{NM}\rangle$ is the NM ground state. Since the pion field is assumed to have zero expectation value in NM, it will be omitted from now on.

The integration over the diquark fields can no longer be done exactly. Here we resort to the stationary phase approximation, where only the terms quadratic in the diquark fields are retained in the quark determinant – i.e., n-point diquark interaction terms (n=4,6,8...) are omitted. After performing the Nambu-Gorkov trace in (3.10), this amounts to the replacement

$$-\frac{i}{2} \text{Tr} \ln S^{-1} - \int d^4x \frac{\Delta_a^* \Delta_a}{4G_s} \rightarrow -i \text{tr} \ln S_0^{-1} + \Delta_a D_0^{-1} \Delta_a^*. \quad (3.14)$$

Here we introduced the following quantities, which we write down in momentum space for further use:

$$D_0(k) = \frac{-4G_s}{1 + 2G_s \Pi_s(k)} \quad (3.15)$$

$$\Pi_s(k) = 6i \int \frac{d^4q}{(2\pi)^4} \text{tr}_D [\gamma_5 S_0(q) \gamma_5 \tilde{S}_0(q-k)] \quad (3.16)$$

$$S_0(k) = \frac{1}{\not{k} - M - \not{\phi}}, \quad \tilde{S}_0(k) = \frac{1}{\not{k} - M + \not{\phi}}. \quad (3.17)$$

⁴The quark mass parameter M is considered as a variable in the effective potential, and its physical value, which is the solution of the gap equation at density $\rho > 0$ ($\rho = 0$), is denoted as M^* (M_0). The same notation will be used for the nucleon mass $M_N = M_N(M)$ and the gap Δ , i.e., their physical values are $M_N^* = M_N(M^*)$ and Δ^* at finite density, and $M_{N0} = M_N(M_0)$ and $\Delta_0 = 0$ at zero density.

Since we wish to construct the nucleon as a quark-diquark state, we will retain the diquark fields to all orders in the first term of (3.11) in order to derive the nucleon propagator in the ladder approximation to the Faddeev equation. To evaluate this term, we need the form of S , which is easily derived by inverting (3.12) – see Appendix A. Since only terms with the same number of Δ 's and Δ^* 's survive after the diquark integration, because of baryon number conservation, the non-diagonal parts of S in Nambu-Gorkov space, which involve unpaired fields Δ or Δ^* , do not contribute. After performing the Nambu-Gorkov trace, we therefore find that the first term in (3.11) becomes effectively (see Appendix A)

$$\frac{1}{3}\overline{\phi}\left(\Delta\frac{S_0}{1+S_0\gamma_5\Delta_{a'}\beta_{a'}\tilde{S}_0\gamma_5\Delta_a^*\beta_a}\Delta^*\right)\phi \quad (3.18)$$

After the integration over the diquark fields the nucleon field becomes a dynamical variable, and this term gives the Faddeev propagator. In order to simplify the formulae, we will refer here only to the “static approximation” to the Faddeev equation [28], which will be used for the numerical calculations in this paper. It is obtained by replacing \tilde{S}_0 , which appears between the diquark fields in the denominator of (3.18) and describes the quark exchange between the diquark and the spectator quark, according to $\tilde{S}_0 \rightarrow -1/M$.⁵

The integration over the diquark fields is performed as usual by treating the sum of the second term in (3.14) and the term in (3.18) proportional to $\Delta\Delta^*$ as the free diquark action

$$\mathcal{S}_{D0} \equiv \Delta_a D^{-1} \Delta_a^* \equiv \Delta_a \left(D_0^{-1} + \frac{1}{3}\overline{\phi} S_0 \phi \right) \Delta_a^*, \quad (3.19)$$

⁵Only in this approximation is the nucleon auxiliary field a local one.

and the remaining part of (3.18) as the interaction part

$$\mathcal{S}_{DI}(\Delta, \Delta^*) = \frac{1}{3} \bar{\phi} \left(\Delta S_0 \frac{\frac{1}{M} (\Delta_{a'} \beta_{a'}) (\Delta_a^* \beta_a)}{1 - \frac{1}{M} S_0 (\Delta_{a'} \beta_{a'}) (\Delta_a^* \beta_a)} S_0 \Delta^* \right) \phi. \quad (3.20)$$

After introducing an auxiliary source term $\Delta_a^* J_a + J_a^* \Delta_a$ into the Lagrangian density to perform the diquark integration, we obtain, with $\mathcal{S}_D \equiv \mathcal{S}_{D0} + \mathcal{S}_{DI}$:

$$\begin{aligned} & \int \mathcal{D}\Delta \int \mathcal{D}\Delta^* \exp(i\mathcal{S}_D) \\ &= \exp\left(-\text{Tr} \ln D_0^{-1}\right) \exp\left(-\text{Tr} \ln \left[1 + \frac{1}{3} D_0 \bar{\phi} S_0 \phi\right]\right) \end{aligned} \quad (3.21)$$

$$\times \left[\exp\left(i\mathcal{S}_{DI} \left(\frac{\delta}{\delta(iJ^*)}, \frac{\delta}{\delta(iJ)}\right)\right) \exp(-iJ_a^* D J_a) \right]_{J=J^*=0} \quad (3.22)$$

Expanding this expression in powers of the nucleon sources gives the nucleon propagator as the coefficient of $\bar{\phi}\phi$, and interactions between nucleons as the higher order terms⁶. Here we concentrate on the nucleon kinetic term. Since the interaction part, Eq.(3.20), contains all powers of the diquark fields, many contractions emerge when the derivatives indicated in (3.22) are carried out, even if we restrict ourselves to the nucleon kinetic term $\propto \bar{\phi}\phi$. A subset of these contractions constitutes the ladder approximation to the Faddeev equation (see Appendix A), which leads to

$$\begin{aligned} & \int \mathcal{D}\Delta \int \mathcal{D}\Delta^* \exp(i\mathcal{S}_D) \\ &= \exp\left(-\text{Tr} \ln D_0^{-1}\right) \exp\left(i\bar{\phi} G_N \phi\right) + \mathcal{O}\left[\left(\bar{\phi}\phi\right)^2\right], \end{aligned} \quad (3.23)$$

where the nucleon (quark-diquark) propagator G_N in the ladder approximation is expressed in terms of the quark-diquark t-matrix (T_N) in momentum

⁶An interesting example is the second exponential factor in (3.21), which describes interactions between nucleons proceeding via quark exchange processes.

space by

$$G_N(p) = \Pi_N(p) + \Pi_N(p)T_N(p)\Pi_N(p) \quad (3.24)$$

$$\Pi_N(p) = i \int \frac{d^4k}{(2\pi)^4} S_0(k) D_0(p-k) \quad (3.25)$$

$$T_N(p) = \frac{-3}{M} \frac{1}{1 + \frac{3}{M} \Pi_N(p)} \quad (3.26)$$

The quark and diquark propagators, D_0 and S_0 , appearing in the quark-diquark bubble graph, (3.25), have been given in Eqs.(3.15) and (3.17).⁷ As explained in sect.2.1.1 of Ref.[17], T_N has a pole at $\not{p}_N = M_N$, where $p_N^\mu = p^\mu - 3\omega^\mu$. If the total system under consideration (nuclear matter) is at rest, the space components of the vector field vanish, and the nucleon positive energy spectrum becomes $\epsilon_N(p) = E_N(p) + 3\omega^0$, with $E_N(p) = \sqrt{\mathbf{p}^2 + M_N^2}$.

Inserting these results obtained above into the effective action of Eq.(3.10), (3.11), and finally integrating over the nucleon sources (see Appendix A), we obtain the effective action for the nucleons in the mean field (Hartree) approximation:

$$\mathcal{S}_{\text{eff}} = -i \left(\text{Tr} \ln S_0^{-1} - \text{Tr} \ln D_0^{-1} - \text{Tr} \ln G_N^{-1} \right) \quad (3.27)$$

$$+ \bar{N} G_N^{-1} N + \int d^4x \left(-\frac{(M-m)^2}{4G_\pi} + \frac{\omega_0^2}{4G_\omega} \right). \quad (3.28)$$

The three “trace-log terms” in (3.27) are the results of the integrations over the quark fields, the diquark fields, and the nucleon sources, respectively. The first term in (3.28) is the kinetic term of the nucleon, and the rest are the c-number terms associated with the mean scalar and vector fields.

⁷The diquark propagator, D_0 , is related to the quantity τ_s of Ref.[17] by $D_0 = i\tau_s$. The t-matrix (3.26) is related to $T(p)$ in Eq.(2.7) of Ref.[17] by $T_N(p) = -T(p)$. We also note that the factor $2G_\omega$ in Eq.(2.8) of the present paper was not included in the definition of the field ω^μ in Ref.[17].

We now introduce a chemical potential (μ) for the nucleon into the kinetic term of (3.28). Before that, however, we note that if one had continued and integrated $\exp(i\mathcal{S}_{\text{eff}})$ over the nucleon fields as well, the last term in (3.27) would cancel with the result of the integration, and one would get an expression which could be obtained directly from (2.6) without any reference to nucleons. This is obvious, since we introduced the nucleon auxiliary fields in (3.9) in order that the generating functional would be unchanged. This observation is important, however, because it means that, as a consequence of the composite nature of the nucleon, there are no nucleon vacuum loop terms. That is, there are no nucleon loop contributions to the effective potential *unless* we introduce a chemical potential into the kinetic energy term of (3.28). The vacuum loop terms are exhausted already by the quark and diquark loops in (3.27), which describe the polarization of the quark Dirac sea and the effects of quark-quark correlations (so called, ring contributions) in the quark Dirac sea, respectively.

Concerning the ring contributions (corresponding to the second term in Eq.(3.27)), we note that meson loops, which were omitted from the outset in our simplified treatment, would give very similar terms. A consistent treatment of the ring contributions would therefore require both meson and diquark loops. This is beyond the scope of the present approximation, where we have retained the diquark fields solely in order to construct the single nucleon as a quark-diquark state. In the framework of the Hartree approximation for the EOS, we therefore drop the second term in Eq.(3.27).

One can rewrite the nucleon kinetic term by introducing a renormalized nucleon field (\hat{N}), such that, near the pole, the renormalized propagator (\hat{G}_N)

behaves as $\hat{G}_N \rightarrow \not{p}_N - M_N$.⁸ The pole part of the nucleon kinetic term including the chemical potential then becomes

$$\overline{N} G_N^{-1} N \rightarrow \overline{\hat{N}} (\not{p} - M_N + \mu^* \gamma^0) \hat{N}, \quad (3.29)$$

where $\mu^* \equiv \mu - 3\omega^0$.

To continue the derivation of the effective potential (V) for NM in the path integral formalism, we finally have to integrate over the nucleon field and express the result as $S_{eff} = -\int d^4x V$, where V is a function of the classical fields M and ω^0 . Combining the result of the integration of the kinetic term (3.29) with the last term of Eq.(3.27), we get the nucleonic contribution to the effective potential⁹

$$V_N = i \int \frac{d^4p}{(2\pi)^4} \text{tr} \ln (\not{p} - M_N + \mu^* \gamma^0) - (\mu = 0 \text{ term}) \quad (3.30)$$

$$\begin{aligned} &= \frac{i}{2} \times 2 \int \frac{d^4p}{(2\pi)^4} \left[\text{tr}_D \ln (-\not{p} - M_N + \mu^* \gamma^0) (\not{p} - M_N + \mu^* \gamma^0) \right] - (\mu = 0 \text{ term}) \\ &= 2i \int \frac{d^4p}{(2\pi)^4} \left[\ln \frac{p_0^2 - (E_N(p) + \mu^*)^2}{p_0^2 - E_N(p)^2} + \ln \frac{p_0^2 - (E_N(p) - \mu^*)^2}{p_0^2 - E_N(p)^2} \right] - (\mu^* \rightarrow -3\omega^0) \end{aligned} \quad (3.31)$$

$$= -4 \int \frac{d^3p}{(2\pi)^3} \Theta(\mu^* - E_N(p)) \cdot (\mu^* - E_N(p)), \quad (3.32)$$

which is nothing but the familiar contribution to the effective potential arising from the nucleon Fermi motion. Adding the quark loop contribution (the first term in (3.27)) and the mean field terms of (3.28), we finally obtain the

⁸Mathematically, we write $N = \sqrt{Z_N} \hat{N}$ and $G_N = Z_N \hat{G}_N$ with $Z_N = -(M/3) \left[(\partial \Pi_N(p_N) / \partial \not{p}_N) \not{p}_{N=M_N} \right]^{-1}$.

⁹For the explicit evaluation of the Dirac determinant, see Appendix B for the case $\Delta = 0$. The trace indicated by the symbol tr does not include the functional trace. The subtraction of the $\mu = 0$ term in (3.30) arises from the last term in (3.27), and the factor 2 in the second line comes from the isospin trace.

effective potential for NM in the form

$$V = V_{\text{vac}} + V_N - \frac{\omega_0^2}{4G_\omega} \quad (3.33)$$

where V_N is given by (3.32), and the vacuum term is

$$V_{\text{vac}} = 12i \int \frac{d^4k}{(2\pi)^4} \ln \frac{k^2 - M^2}{k^2 - M_0^2} + \frac{(M - m)^2}{4G_\pi} - \frac{(M_0 - m)^2}{4G_\pi}. \quad (3.34)$$

Here we subtracted the zero density contribution ($M = M_0$). The values of ω_0 and M for fixed μ are determined by the equations¹⁰ $\partial V / \partial \omega = \partial V / \partial M = 0$. The pressure as a function of μ is then obtained as $P = -V$. The baryon density follows from $\rho = -\partial V / \partial \mu$, and the energy density is given by $\mathcal{E}(\rho) = V + \mu\rho$.

The effective potential (3.33) differs from the familiar expression in the linear sigma model for point-nucleons [29] only through the dependence of the nucleon mass M_N on the mean scalar field (or, equivalently, on M). Since the scalar field now couples to the quarks in the nucleon instead of an elementary nucleon, the function $M_N(M)$, which is determined by the pole position of the quark-diquark t-matrix (3.26), is in general a non-linear function of M . If it has a large positive curvature (scalar polarizability), the binding energy per nucleon saturates, as has been discussed in detail in Ref.[17].

3.2 Color superconducting quark matter

To obtain the EOS of QM in the Hartree approximation, we introduce a chemical potential for quark number $\mu_q = \mu/3$ into the Lagrangian density

¹⁰In principle, the quantity which has to be minimized is the effective potential after Wick rotation. In this case the last term in Eq.(3.33) changes its sign, and the physical value of ω_0 is a minimum of V .

(2.6), and assume that the fields Σ , ω^0 and Δ_{11} have finite expectation values. The choice $D = 1$ for the diquark field Δ_{Da} corresponds to a special choice of the phase and breaks the $U(1)$ symmetry, while the choice $a = 1$ breaks the color $SU(3)$ symmetry down to $SU(2)$ ¹¹. Since we do not consider fluctuations of the bosonic fields in this work, it is sufficient to use the following Lagrangian density:

$$\mathcal{L} = \bar{\Psi} S^{-1} \Psi - \frac{(M - m)^2}{4G_\pi} + \frac{\omega_0^2}{4G_\omega} - \frac{\hat{\Delta}^2}{4G_s}. \quad (3.35)$$

Here

$$S^{-1} = i\not{\partial} - M + \mu_q^* \gamma^0 \sigma_3 - i\gamma_5 \sigma_1 \hat{\Delta} \beta_1, \quad (3.36)$$

where $\mu_q^* = \mu_q - \omega_0$, and the meson mean fields are defined in terms of the ordinary quark fields $\bar{\psi}$, ψ by (compare with Eqs. (2.7), (2.8), and (3.13))

$$\begin{aligned} M &= m - 2G_\pi \langle \text{QM} | \bar{\psi} \psi | \text{QM} \rangle, & \omega_0 &= 2G_\omega \langle \text{QM} | \psi^\dagger \psi | \text{QM} \rangle, \\ \hat{\Delta} &= -2G_s \frac{1}{2} \langle \text{QM} | (\bar{\psi} i\gamma_5 \beta_1 C \tau_2 \bar{\psi}^T - \psi^T C^{-1} \tau_2 i\gamma_5 \beta_1 \psi) | \text{QM} \rangle. \end{aligned} \quad (3.37)$$

The poles of the quark propagator, S , are easily determined by inverting Eq.(3.36). There are 4 poles, at $p_0 = \pm \sqrt{(E_q(p) \pm \mu^*)^2 + \Delta^2}$, each with degeneracy 8, and 4 poles at $p_0 = \pm |E_q(p) \pm \mu^*|$, each with degeneracy 4. Here $E_q(p) = \sqrt{\mathbf{p}^2 + M^2}$, and $\Delta \equiv \sqrt{\frac{3}{2}} \hat{\Delta}$.

¹¹There are 5 different Goldstone bosons corresponding to these broken symmetries. If we start from the $(\sigma_1 \beta_1)$ mode (Δ_{11}), which characterizes the ground state, the $U(1)$ phase rotation mixes in the $(\sigma_2 \beta_1)$ mode, and the color $SU(3)$ rotation mixes in the $(\sigma_1 \beta_2)$, $(\sigma_1 \beta_3)$ and $(\sigma_2 \beta_a)$ ($a = 1, 2, 3$) modes, which correspond to the Goldstone bosons. Note that the $(\sigma_2 \beta_1)$ mode is mixed into the ground state by both phase and color rotations. The quark-quark t-matrices in these channels have zero energy poles. For comparison, we note that the familiar Goldstone pion in the present Nambu-Gorkov formalism emerges as a σ_3 -mode in the $(0^-, T = 1)$ color singlet channel, which is mixed into the σ_1 -mode in the $(0^+, T = 0)$ color singlet channel of the ground state by the chiral rotation.

Integration over the quark fields gives a contribution $-\frac{i}{2}\text{Tr} \ln S^{-1}$ to the effective action, which can be evaluated (Appendix B) with the result

$$\begin{aligned}
-\frac{i}{2}\text{Tr} \ln S^{-1} = & - \int d^4x \\
& \times 2i \int \frac{d^4p}{(2\pi)^4} \left[2 \ln \left(p_0^2 - (E_q(p) + \mu_q^*)^2 - \Delta^2 \right) + 2 \ln \left(p_0^2 - (E_q(p) - \mu_q^*)^2 - \Delta^2 \right) \right. \\
& \left. + \ln \left(p_0^2 - (E_p + \mu_q^*)^2 \right) + \ln \left(p_0^2 - (E_p - \mu_q^*)^2 \right) \right]. \quad (3.38)
\end{aligned}$$

If we separate the contributions surviving for $\Delta = 0$, we finally obtain the following form of the effective potential for QM (compare to (3.33) for the NM case):

$$V = V_{\text{vac}} + V_Q + V_\Delta - \frac{\omega_0^2}{4G_\omega} \quad (3.39)$$

where V_{vac} has the same form as in nuclear matter (see Eq.(3.34)), V_Q is the contribution of the quark Fermi motion given by

$$V_Q = -12 \int \frac{d^3p}{(2\pi)^3} \Theta(\mu_q^* - E_q(p)) (\mu_q^* - E_q(p)), \quad (3.40)$$

and V_Δ is the contribution arising from the finite gap:

$$\begin{aligned}
V_\Delta = & 4i \int \frac{d^4p}{(2\pi)^4} \left[\ln \frac{p_0^2 - (E_q(p) + \mu_q^*)^2 - \Delta^2}{p_0^2 - (E_q(p) + \mu_q^*)^2} + \ln \frac{p_0^2 - (E_q(p) - \mu_q^*)^2 - \Delta^2}{p_0^2 - (E_q(p) - \mu_q^*)^2} \right] \\
& + \frac{\Delta^2}{6G_s}. \quad (3.41)
\end{aligned}$$

The values of ω_0 , M and Δ for fixed chemical potential are obtained by solving the equations $\partial V / \partial \omega_0 = \partial V / \partial M = \partial V / \partial \Delta = 0$. (Concerning the dependence on ω_0 , see the last footnote in subsect.3.1.) The pressure, baryon density and energy density are then obtained from $P = -V$, $\rho = -\frac{\partial V}{\partial \mu}$, and $\mathcal{E} = V + \mu\rho$, where $\mu = 3\mu_q$ is the chemical potential for baryon number as before.

4 Numerical results

In the numerical calculations discussed below, the proper time regularization scheme will be used. In this scheme, one performs a Wick rotation of the energy variable of the loop integral, and then introduces the replacements

$$\ln A \rightarrow \int_{1/\Lambda_{\text{UV}}^2}^{1/\Lambda_{\text{IR}}^2} \frac{d\tau}{\tau} e^{-\tau A}, \quad \frac{1}{A^n} \rightarrow \frac{1}{(n-1)!} \int_{1/\Lambda_{\text{UV}}^2}^{1/\Lambda_{\text{IR}}^2} d\tau \tau^{n-1} e^{-\tau A} \quad (n \geq 1), \quad (4.42)$$

where A depends on the momenta and, possibly, Feynman parameters, and Λ_{UV} and Λ_{IR} denote the UV and IR cut-offs, respectively.

As discussed in detail in Ref.[17], the validity of the “static approximation” to the Faddeev equation, which leads to the contact-type quark-diquark interaction $\propto 1/M$ in the t-matrix (3.26), breaks down as M decreases with increasing density, and leads to large deviations from the exact Faddeev results for the function $M_N(M)$. On the other hand, it was shown that if one fixes the quark-diquark interaction to its value at zero density ($1/M \rightarrow 1/M_0$ in the denominator of Eq.(3.26)), the exact Faddeev results are qualitatively reproduced. Furthermore, if one uses an interpolating form of the quark-diquark interaction ($1/M \rightarrow (1/M_0)(M_0 + c)/(M + c)$, with $c = 0.7$ GeV, in the denominator of (3.26)), the agreement is very good. We will use this interpolating form in the following calculations.

4.1 EOS of NM

In order to provide a basis for our later discussions on the NM \rightarrow QM phase transition, we first reproduce in Figs. 1 and 2 the results obtained in Ref.[17] for the nucleon mass as a function of the scalar potential, $M - M_0$, as well as

the binding energy per nucleon as a function of density. The parameters used in this calculation are shown in Table 1. For the choice $\Lambda_{IR} = 0$ there is an unphysical threshold for the decay of the nucleon into a quark and a diquark, and the function $M_N(M)$ cannot develop a sufficiently large curvature (scalar polarizability), which is required to stabilize the system. In contrast, for the case $\Lambda_{IR} = 0.2$ GeV the nucleon mass exceeds the would-be threshold for large scalar potentials, leading to a sufficiently large scalar polarizability and to saturation of the binding energy¹². The effective masses of the nucleon and the quark for the case $\Lambda_{IR} = 0.2$ GeV are shown by the solid lines in Fig. 3. We observe that there is only a limited tendency toward chiral restoration in NM. The pressure of NM will be discussed later in connection with the phase transition to QM.

Let us discuss here another aspect which provides a further illustration of the importance of avoiding unphysical decay thresholds, namely the mass of the ω -meson in NM. We take the simplest case of an ω -meson at rest ($\mathbf{q} = 0$), and consider the pole position $q_0 \equiv M_\omega^*$ of the effective NN interaction in the t-channel with quantum numbers 1^+ . The effective NN interaction for the case $\mathbf{q} = q_0 = 0$ is the familiar Landau-Migdal interaction, which was derived in Ref.[17] directly from the expression for the NM energy density. The part associated with the spatial components of the exchanged ω -meson has the

¹²We recall from Ref.[17] that the only free parameter for the calculation of the NM EOS, r_ω , has been adjusted so that the binding energy curve passes through the empirical saturation point. That is, with the limited number of parameters in this simple NJL model, it is not possible to ensure that the calculated saturation point agrees with the empirical one.

form ¹³

$$f_\omega(\mathbf{p}', \mathbf{p}) = -\frac{18 G_\omega}{1 + 18 G_\omega \frac{\rho}{E_F^*}} \frac{\mathbf{p}' \cdot \mathbf{p}}{E_N^*(p') E_N^*(p)}, \quad (4.43)$$

where $E_F^* = \sqrt{p_F^2 + M_N^{*2}}$. The part involving $18 G_\omega \frac{\rho}{E_F^*}$ is a density dependent N-loop contribution – i.e., the Fermi average over the Z-graph for external vector fields with zero momentum. (This is the same type of medium correction which reduces the enhanced isoscalar magnetic moments in relativistic many-nucleon theories [30].)

Since the nucleon remains a rather massive object even at finite density (see Fig. 3), we can expect that for the case of finite energy transfer this N-loop contribution will not depend very strongly on q_0 , and we therefore approximate it here by its value at $q_0 = 0$. Then, for finite q_0 , the only additional contribution arises from the exchange of $q\bar{q}$ pairs in the t-channel, described by the transverse part of the polarization (bubble graph) Π_ω – see Appendix C. The constant in the denominator of Eq.(4.43) is then replaced according to

$$18 G_\omega \frac{\rho}{E_F^*} \longrightarrow 18 G_\omega \frac{\rho}{E_F^*} + 2G_\omega \Pi_\omega(q_0). \quad (4.44)$$

The two terms on the r.h.s. of Eq.(4.44) work in opposite directions for increasing density; the N-loop term represents the effect of the Pauli exclusion principle acting on the nucleons and tends to make the ω -meson heavier, while the $q\bar{q}$ excitation piece tends to make the ω -meson lighter (since the mass of the $q\bar{q}$ pair is reduced).

Using the density dependent quark mass in NM, as shown in Fig. 3, and the value of r_ω from Table 1, we obtain the result for M_ω^* shown in Fig. 4.

¹³See Eq.(2.50) of Ref.[17]. We note that the factor $\frac{1}{2}$ appearing there in the denominator is a misprint. The correct expression is (4.43).

First we note that r_ω has been adjusted in Ref.[17] so that the binding energy curve passes through the empirical saturation point. From Fig. 4 we see that this leads to an ω meson mass of 827 MeV at zero density, which is larger than the experimental value of 783 MeV, but nevertheless reasonable. Second, the ω meson mass decreases by about 80 MeV at normal NM density and by about 120 MeV for $\rho \simeq 0.5 \text{ fm}^{-3}$. For higher densities it increases slightly because of the increasing importance of Pauli blocking¹⁴. In comparison with our earlier NJL model calculations, we note that the overall picture for the ω -meson mass is similar to that for the σ -meson mass (see Fig. 11 of Ref.[17]), and also to the nucleon and quark masses shown in Fig. 3. That is, the density dependence is rather mild, and there are no sudden changes of the behavior at high density. Third, we note that the ω meson mass shown in Fig. 4 is always above the would-be $q\bar{q}$ threshold. If we set $\Lambda_{\text{IR}} = 0$, leaving the other parameters unchanged, we would still get a bound state at zero density ($M_\omega = 780 \text{ MeV}$), but this state would already dissolve at $\rho \simeq 0.04 \text{ fm}^{-3}$, because of the decreasing $q\bar{q}$ threshold. Once again this shows the importance of avoiding the unphysical threshold in the NM calculation.

4.2 EOS of QM without the effect of diquark condensation

The effective quark mass in QM is shown as a function of the density by the dashed line in Fig. 3. The parameters used in this calculation are the same as for NM, see Table 1. (We note that the value of r_ω has no influence on

¹⁴In view of the interest in searching for possible bound ω -nucleus states [18], it is interesting to note that these results are very close to those found in the quark meson coupling model [19], with the ω -meson being somewhat less bound than it would be in Walecka-type models [20].

M^* .) The sharp decrease of M^* in QM around 0.3 fm^{-3} reflects the well known chiral phase transition which would happen for the case $m = 0$ ¹⁵. We see that the NM and QM cases are qualitatively very different and one should not treat ordinary finite density matter as QM.

Fig. 5 shows the variation of the pressure as a function of the chemical potential for NM (solid line), and for QM with the same model parameters as for NM (dashed line labeled by $r_\omega = 0.37$), as well as for the choice $r_\omega = 0$ (dashed line labeled by $r_\omega = 0$). The case of zero density corresponds to the point $(P, \mu) = (0, M_{N0})$ for NM, and to $(0, 3M_0)$ for QM, where $M_{N0} = 940 \text{ MeV}$ and $M_0 = 400 \text{ MeV}$ are the zero density values of the nucleon and constituent quark masses. Starting from this point, the density increases along the lines. The vacuum solution $P = 0$, which corresponds to a minimum of the effective potential for $\mu < M_{N0}$ in NM, and for $\mu < 3M_0$ in QM, is not shown in this plot. For a qualitative understanding of our following discussions it is helpful to recall that attractive effects, which soften the EOS, make the $P(\mu)$ curves steeper, and repulsive effects make them flatter.

Let us first summarize some well known points concerning the phase transitions which occur within the NM and QM phases separately. In the region below the saturation density, the NM EOS shows the familiar behavior of a first order gas-liquid phase transition, which is shown in more detail in the insert of Fig. 5. The pressure decreases with increasing density until it reaches a minimum at some density ρ_c , and then it increases and passes through $P = 0$ at the saturation density ρ_0 . In other words, for densities between ρ_c and ρ_0 there are 3 extrema of the effective potential as a function

¹⁵Since in the numerical calculations of this paper we always adjust the parameters so as to reproduce the experimental pion mass, we refer to this kind of behavior as the “would-be chiral phase transition”, or simply the “chiral phase transition”.

of M , corresponding to (i) a maximum at negative pressure corresponding to unstable NM droplets, (ii) the NM phase, which has negative pressure for $\rho < \rho_0$ (quasi-stable NM droplets), and positive pressure for $\rho > \rho_0$ (stable NM), and (iii) the vacuum phase ($P = 0$), which is the ground state (state with the largest pressure) for $\rho < \rho_0$.

The EOS of QM for the case $r_\omega = 0$ has a bound state, and in this case the behavior is qualitatively similar to that of NM, discussed above. The gas-liquid phase transition of NM now corresponds to the familiar first order chiral phase transition in QM, where the unstable branch with decreasing pressure is characterized by massive constituent quarks (broken chiral symmetry), and the metastable ($P < 0$) and stable ($P > 0$) branches with increasing pressure correspond to the chirally restored phase. The first order phase transition occurs at $P = 0$ in this case, but if one increases r_ω the curve will cross itself at finite P , and a further increase of r_ω leads to a chiral phase transition of second order, as shown for $r_\omega = 0.37$ in Fig. 5. In this case there is only one minimum of the effective potential as a function of M for any given μ , and at some μ the maximum at $M \simeq 0$ turns into a minimum. The density increases along the dashed line for $r_\omega = 0.37$, starting at the point where $\mu = 3 M_0 = 1200$ MeV and $P = 0$, and at $\mu = 1500$ MeV ($\rho = 0.41$ fm $^{-3}$) the quark effective mass is already as small as $M^* = 53$ MeV.

The branch of the QM EOS corresponding to (almost) massless quarks is essentially the EOS of a free massless quark gas [4]. This is demonstrated by the dotted lines in Fig.5, which show the EOS for a massless quark gas for two choices of the bag constant B : $B_{\text{NJL}} = 139.7$ MeV fm $^{-3}$ is the height of the Mexican hat vacuum potential (3.34) at $M = 0$, and $B_{\text{MIT}} = 57.5$ MeV fm $^{-3}$ is the value used in the MIT bag model. By comparing the dashed line for

$r_\omega = 0$ with the dotted line for $B = B_{\text{NJL}}$, we see that, in the region which is relevant for a discussion of the NM \rightarrow QM phase transition, one could neglect the spontaneous breaking of chiral symmetry from the outset and start with massless quarks.

By comparing the solid line with the dashed line for the case $r_\omega = 0.37$ in Fig. 5, we see that there is no NM \rightarrow QM phase transition if we use the same model parameters to describe the two phases. That is, NM would be the ground state for all densities. It will be demonstrated later that this unsatisfactory situation cannot be improved by including the possibility of diquark condensation. (A stiffer EOS for NM would certainly come closer to the QM result at high densities, but one never gets a crossing for any reasonable NM EOS.) On the other hand, the dashed curve with $r_\omega = 0$ is much closer to the NM curve, although still there is no phase transition. However, it will be shown below that this situation changes immediately if one allows for the possibility of diquark condensation.¹⁶ We conclude from Fig. 5 that it is not possible to get a phase transition from NM to normal QM by using the same parameters for the description of the two phases, in particular the same strength of the vector interaction. This point was also noted in a recent investigation [32]. However, if one uses $r_\omega = 0$ in QM and further considers effects which soften the QM EOS, like diquark or pion condensation, there could be a phase transition.

Based on the preceding discussion, we are led to consider the question of whether it is reasonable to use the same model parameters for NM and QM or not. Two among the parameters listed in the second column of Table 1

¹⁶We also note that the dotted line labeled by $B = B_{\text{MIT}}$ in Fig. 5, which has only little to do with the NJL model, crosses the NM line in the high density region, but there is also an unphysical crossing in the low density region.

have been fixed by considering only the properties of NM, namely Λ_{IR} and r_ω . First, one needs a finite IR cut-off in order to describe a stable NM state, but the results are rather insensitive to its actual value as long as $\Lambda_{\text{IR}} > 0.1$ GeV. The introduction of a finite Λ_{IR} takes into account one aspect of confinement physics, which is important for single hadrons and NM. However, there is no reason a priori to introduce an IR cut-off in QM. On the contrary, one might expect that quark decay processes are welcome in this case, and that the choice $\Lambda_{\text{IR}} = 0$ would be more reasonable. Second, one also needs a finite value of r_ω in NM in order to reproduce the saturation properties. Once again, there is no compelling reason to use the same value in QM, and from Fig. 5 we see that the QM EOS depends very sensitively on the actual value of r_ω .

In order to shed some light on the question of which values of Λ_{IR} and r_ω are reasonable in QM, we return to the problem of the ω meson mass as an example, and investigate whether or not there is a pole corresponding to the ω meson in the $q\bar{q}$ t-matrix in QM. Contrary to the NM case discussed in the previous subsection, we now have a chemical potential for the quarks, which leads to a modification of the $q\bar{q}$ bubble graph arising from Pauli blocking. (The detailed formulae are given in Appendix C.) Fig. 6 shows the situation for the choice $\Lambda_{\text{IR}} = 0.2$ GeV in QM. The would-be threshold, which is $2\sqrt{p_F^2 + M^{*2}}$, is shown as a function of density by the dashed line, and the pole positions for $\mathbf{q} = 0$ are shown for various values of r_ω by the solid lines¹⁷. We see that poles exist even for very small values of the coupling constant.

¹⁷The density dependence shown by the dashed line reflects the behavior of the chemical potential μ_q^* , see the dashed line for $r_\omega = 0$ in Fig. 5. The decrease of M^* with increasing density lowers the threshold, while the effect of Pauli blocking raises the threshold. In the low density region the first effect dominates, while in the high density region, where

We expect that the existence of a hadron pole in QM for all densities is not restricted to the case of the ω meson shown here, but can be ascribed to the finite IR cut-off. This observation indicates that it is not reasonable to use a finite IR cut-off in QM. (Another argument in favor of the choice $\Lambda_{\text{IR}} = 0$ will be given in the next subsection.)

Fig. 7 shows the situation for the case $\Lambda_{\text{IR}} = 0$ in QM. We see that for the choice $r_\omega = 0.37$ there is again a pole for all densities, which now is below the threshold. If the value of r_ω is decreased, the pole disappears in the low density region, but at high densities it re-appears because of the increasing threshold. For $r_\omega = 0.17$ the pole exists only for $\rho > 0.8 \text{ fm}^{-3}$. Since the appearance of a meson pole in high density QM, which was not present in the vacuum, is physically unreasonable, Fig. 7 indicates that one should really set $r_\omega = 0$ in QM.

Based on these discussions, we will use $\Lambda_{\text{IR}} = 0$ and $r_\omega = 0$ in QM in our following discussions. The corresponding parameter set is shown in the third column of Table 1. As compared to the case $\Lambda_{\text{IR}} = 0.2 \text{ GeV}$, there are small changes in m , G_π and Λ_{UV} in order to reproduce the same input values $m_\pi = 140 \text{ MeV}$, $f_\pi = 93 \text{ MeV}$ and $M_0 = 400 \text{ MeV}$. We will investigate the dependence of the QM results on the pairing strength, and therefore we treat r_s as a free parameter in QM. (Some numerical results obtained by using the same values of Λ_{IR} and/or r_ω as for NM are shown in Appendix D.)

the quarks are practically massless, the Pauli effect leads to a continuous increase of the threshold. Figs. 6 and 7 show that the density dependence of the pole positions follows the behavior of the dashes lines

4.3 EOS of QM including the effect of diquark condensation

The effect of diquark condensation on the QM EOS is represented by the piece (3.41) of the effective potential. In order to discuss the nature of the phase transition to the color symmetry broken phase, it is useful to look at the gap equation $\frac{\partial V}{\partial \Delta} = 0$ for fixed M . Besides the trivial solution $\Delta = 0$, the nontrivial solution is obtained by solving the equation

$$1 = f(\Delta^2), \quad (4.45)$$

where the explicit form of the function $f(\Delta^2)$ in the proper time regularization scheme is

$$f(\Delta^2) = \frac{12G_s}{\pi^3} \int_0^\infty dk_0 \int_0^\infty k^2 dk (F_+ + F_-), \quad (4.46)$$

where

$$F_\pm = \frac{\exp\left(-\frac{k_0^2 + \epsilon_\pm^2}{\Lambda_{UV}^2}\right) - \exp\left(-\frac{k_0^2 + \epsilon_\pm^2}{\Lambda_{IR}^2}\right)}{k_0^2 + \epsilon_\pm^2} \quad (4.47)$$

with $\epsilon_\pm^2 = (E_q(k) \pm \mu_q^*)^2 + \Delta^2$. It is easy to show that $f(\Delta^2)$ is a monotonically decreasing function of Δ^2 . For the case $\Lambda_{IR} > 0$, its value at $\Delta^2 = 0$ is finite, and therefore we have one unique nontrivial solution if $f(0) > 1$. In other words, for the case $\Lambda_{IR} > 0$ there exists a threshold value of the chemical potential (for fixed coupling constant G_s), or of the coupling constant G_s (for fixed chemical potential), below which we have only the trivial solution $\Delta = 0$, and above which there is one unique minimum at $\Delta > 0$. The transition to the color broken phase is therefore of second order in this case. On the other hand, for $\Lambda_{IR} = 0$, the function $f(\Delta^2)$ has a logarithmic singularity for $\Delta^2 \rightarrow 0$, and therefore the nontrivial solution exists for all

values of the chemical potential and of the coupling constant. In equations, if $\Lambda_{IR} = 0$ the behavior for small $\Delta \rightarrow 0$ is expressed as follows:

$$f(\Delta^2) = -\frac{6G_s}{\pi^2} p_F \mu_q^{*2} \ln \Delta^2 + \dots \quad (4.48)$$

$$\Delta \propto \exp\left(-\frac{\pi^2}{12G_s p_F \mu_q^*}\right), \quad (4.49)$$

where $p_F \equiv \sqrt{\mu_q^{*2} - M^2}$. In this case, V_Δ has the Mexican hat shape for all values of μ_q^* and G_s , and the system is always in the color symmetry broken phase. This behavior, which is very familiar from ordinary BCS theory [31], can be derived directly from QCD without using an effective quark theory [33]. This observation further supports our choice $\Lambda_{IR} = 0$ in QM.

In Fig. 8 we show the $P - \mu$ plots. The dotted line ($r_s = 0$) is very similar to the corresponding line ($r_\omega = 0$) of Fig. 5, and shows that there is no phase transition from NM to normal QM. However, the softening of the QM EOS arising from diquark condensation leads to a first order phase transition, even for relatively small values of r_s . For example, for $r_s = 0.1$ the phase transition appears only at extremely high densities, but for $r_s = 0.15$ the phase transition sets in at 0.72 fm^{-3} in NM, and ends at 1.21 fm^{-3} in QM. The corresponding transition densities for $r_s = 0.2$ are 0.57 fm^{-3} and 0.95 fm^{-3} . For the case $r_s = 0.25$ the transition densities are already somewhat too low (0.42 fm^{-3} and 0.77 fm^{-3}), and $r_s = 0.3$ is definitely too strong since QM would be the ground state for practically all densities. One should also note that, for any reasonable scenario, those parts of the QM curves which reflect the chiral phase transition are always below the NM curve. The chiral phase transition in QM is therefore not very relevant for the discussion of the $\text{NM} \rightarrow \text{QM}$ phase transition, and one could set $M \equiv 0$ in QM from the beginning with practically identical conclusions.

In Fig. 9 we show the quark effective masses as functions of the density for the same values of r_s as in Fig. 8, and in Fig. 10 we show the gaps as functions of the density. The behaviors of the curves $M^*(\rho)$ still reflect the chiral phase transition in QM, although the density region where M^* varies rapidly is shifted upward compared to the case $r_s = 0$. Fig. 10 shows that the gaps in the present calculation are rather large. In the density region where QM becomes the ground state the gap is of the order of 150 MeV to 250 MeV for those values of r_s which give reasonable transition densities. This figure also supports the conclusion drawn from Fig. 8 that $r_s = 0.3$ is already too strong, since the gap would exceed 300 MeV in the high density region, which is definitely too large.

With regard to the dependence of the above results on the pairing strength, r_s , we would like to make two remarks. The first one concerns the regularization scheme. If we compare, for example, the present proper time scheme to the sharp 3-momentum cut-off scheme, a glance at Table 1 of Ref.[17] shows that the coupling constant G_π in the proper time scheme is almost three times as large as the one in the 3-momentum cut-off scheme. Therefore, for a given value of r_s , the actual value of the coupling constant, G_s , in the proper time scheme is much larger than in the 3-momentum cut-off scheme, which partially explains why our gaps are larger than in previous works [7]. One also has to note that the most important contributions to the gap equation (4.45) come from the region $|\mathbf{k}| \simeq \mu_q^*$ – see Eqs.(4.46) and (4.47). In the high density region, this is of the same order as the UV cut-off in the 3-momentum scheme, and therefore the peak contributions to the gap equation are cut out artificially. On the other hand, the proper time scheme introduces a smooth cut-off function, and the gap can become quite large in

the high density region.

The second remark is that the value $r_s = 0.51$, obtained by fitting the nucleon mass in the pure quark-scalar diquark model, leads to unphysical results in QM. Here again we face the problem that the parameters which work for the nucleon and NM lead to unphysical results when used in QM. However, we believe that for the case of r_s the reason is more simple. The pure quark-scalar diquark model attributes the whole attraction in the 3-quark system to the scalar diquark correlations, whereas it is known that there are other important attractive effects, such as pion exchange [34, 35]. Indeed, it has been shown in Ref.[36] that the inclusion of pion exchange leads to a large reduction of r_s in order to reproduce the experimental nucleon mass. The axial vector diquark channel also leads to some reduction of r_s [9]. It therefore seems that $r_s = 0.51$ is actually an overestimate, and if r_s is determined by using a more complete model for the nucleon, it might also work in the QM calculation.

Let us now illustrate the NM \rightarrow QM phase transition, taking the case $r_s = 0.2$ of Fig. 8 as an example. Since for a given μ the actual ground state of the system is the state with the largest pressure, we see from Fig. 8 (and the insert shown in Fig. 5) that below the NM saturation point the vacuum (VAC) is the ground state, and then the phase transitions to NM and QM occur successively. Since both phase transitions are of first order, the chemical potential is continuous, but the density is discontinuous across the transitions. In Fig. 11 we show the density of the ground state as a function of μ . The density jump for the NM \rightarrow QM transition is quite large, about 0.4 fm^{-3} . Fig. 12 shows the constituent quark mass and the gap of the ground state as functions of μ . This figure illustrates again that the NM

state shows only little tendency toward chiral symmetry restoration, and the transition leads to a QM state which is (almost) chirally symmetric, but where the color symmetry is strongly broken. In Figs. 13 and 14 we show the pressure and the energy density of the ground state as functions of the density. In the mixed phases, which are indicated by the dashed lines, the pressure is constant and the energy density increases linearly with density.

5 Summary and conclusions

In order to discuss the behavior of baryonic matter over a wide range of densities, one has to describe the single hadron, normal saturating nuclear matter, and high density quark matter at the same time. In this paper we have shown a consistent formulation and a feasible numerical treatment of these three aspects, which makes use of the quark-diquark picture for the single nucleon and the Hartree approximation for the many-body systems. We used the NJL model as an effective quark theory, since this model seems to be a unique candidate to provide a simultaneous covariant description of all three aspects of the problem. We paid special attention to the question of those conditions under which a phase transition from nuclear to quark matter becomes possible.

For the description of normal saturating nuclear matter, there are two important ingredients in the NJL model. First, one has to take into account one aspect of confinement physics, namely the absence of unphysical thresholds for the decay into quarks. In the NJL model this can be realized by introducing an infrared cut-off in the framework of the proper time regularization scheme. Only if these unphysical thresholds are avoided, can one describe

normal saturating nuclear matter and stable hadrons in the medium. Second, the vector interaction leads to a repulsion between the nucleons which is inevitable for describing saturation.

These two ingredients are very important in nuclear matter, but it is not clear a priori whether they simply can be taken over to quark matter. In this paper we presented arguments which indicate that it is preferable to use no infrared cut-off and no vector interaction in the high density quark phase.¹⁸ First, the use of an infrared cut-off would lead to hadronic poles for all densities in quark matter, and to a threshold behavior of the gap for small pairing strength and/or small chemical potential, which contradicts the results obtained on more general grounds. It is therefore preferable to use no infrared cut-off in quark matter. Second, the use of the same vector interaction as in nuclear matter would lead to ω meson poles in the high density region of quark matter.

After the discussion of these points, we turned the problem of the phase transition from nuclear matter to normal quark matter. We found that there is no phase transition at all – i.e., nuclear matter is the ground state for all densities. We then took into account the effect of scalar diquark condensation in quark matter, treating the 4-fermi coupling constant in this channel (the pairing strength) as a free parameter. We found that the quark matter equation of state is softened considerably, even for relatively small pairing strengths, leading to a first order phase transition from nuclear matter to

¹⁸We remind the reader that, concerning the equation of state of high density quark matter, the value of the infrared cut-off has no strong influence on the results, but the strength of the vector interaction is crucial. There would be no phase transition from nuclear matter to quark matter if one used the same strength of the vector interaction for the description of the two phases.

quark matter at a transition density which decreases with increasing pairing strength. That is, in our calculation there is a phase transition from nuclear matter to superconducting quark matter, but no phase transition to normal quark matter. The ground state of the system is then nuclear matter at normal densities, where chiral symmetry is strongly broken and color symmetry is intact, and quark matter at high densities, where chiral symmetry is almost restored and color symmetry is strongly broken. We illustrated this picture by using an explicit numerical example in our model calculation.

The results discussed in this paper for the equations of state of nuclear matter and quark matter show that, in many respects, these two systems have very different properties. In order to discuss the phase transition more quantitatively, it is important to account for these differences in the framework of an effective theory which is able to describe both phases consistently.

ACKNOWLEDGEMENT

This work was supported by the Grant in Aid for Scientific Research of the Japanese Ministry of Education, Culture, Sports, Science and Technology, Project No. C2-13640298, the Australian Research Council and The University of Adelaide.

References

- [1] Proc. Int. Workshop on *Compact Stars in the QCD Phase Diagram* (Copenhagen, Aug. 2001), **eConf C010815** (2002); [Contributions of M. Alford (hep-ph/0110150), G.W. Carter (hep-ph/0111353), etc.];
Proc. ECT* Int. Workshop on *Physics of Neutron Star Interiors* (NSI00), Lect. Notes Phys. **578** (2001); [Contributions of T. Schäfer and E. Shuryak (nucl-th/0010049), etc.];
J.J. Drake et al., *Astrophys. J.* **572** (2002) 996;
R. Sharma and S. Mukerjee, *Mod. Phys. Lett. A* **16** (2001) 1049;
K. Yamaguchi, M. Iwasaki and O. Miyamura, *Prog. Theor. Phys.* **107** (2002) 117;
M. Alford and K. Rajagopal, hep-ph/0204001;
D. Blaschke, T. Klähn and D.N. Voskresensky, *Ap. J.* **533** (2000) 406.
- [2] International Workshop on *Quark and Hadron Dynamics* (Budapest, March 2002); [Contributions of T. Csörgö and A. Ster (nucl-th/0207016), etc];
Proc. 15th Int. Conference on *Ultrarelativistic Nucleus-Nucleus Collisions* (QM2001), *Nucl. Phys. A* **698** (2002).
- [3] P. A. Guichon, K. Saito, E. N. Rodionov and A. W. Thomas, *Nucl. Phys. A* **601**, 349 (1996)
- [4] J. Cleymans, R.V. Gavai and E. Suhonen, *Phys. Rep.* **130** (1986) 217;
N.K. Glendenning, *Nucl. Phys. A* **512** (1990) 737.
- [5] D. Bailin and A. Love, *Phys. Rep.* **107** (1984) 325;
T. Schäfer, *Nucl. Phys. A* **642** (1998) 45; *Int. J. Mod. Phys. B* **15** (2001)

- 1474;
R.D. Pisarski and D.H. Rischke, Phys. Rev. **D 60** (1999) 094013; Phys. Rev. **D 61** (2000) 074017;
Proc. 5th Int. Workshop on *QCD* (QCD2000), World Scientific, Singapore, 2001 (eds. B. Müller and Y. Gabellini).
- [6] K. Iida and G. Baym, Phys. Rev. **D 65** (2002) 014022; hep-ph/0204124;
P. Amore, M. Birse, J.A. McGovern and N.R. Walet, Phys. Rev. **65** (2002) 074005;
P.F. Bedaque and T. Schäfer, Nucl. Phys. **A 697** (2002) 802;
V.P. Gusynin and I.A. Shovkovy, Nucl. Phys. **A 700** (2002) 577;
H. Abuki, T. Hatsuda and K. Itakura, Phys. Rev. **D 65** (2002) 074014.
- [7] M. Alford, K. Rajagopal and F. Wilczek, Phys. Lett. **B 422** (1998) 247;
J. Berges and K. Rajagopal, Nucl. Phys. **B 538** (1999) 215;
R. Rapp, T. Schäfer, E.V. Shuryak and M. Velkovsky, Phys. Rev. Lett. **81** (1998) 53;
O. Kiriya, S. Yasui and H. Toki, Int. J. Mod. Phys. **E 10** (2001) 501.
- [8] F.E. Close and A.W. Thomas, Phys. Lett. **B 212** (1988) 227;
A.W. Schreiber, A.I. Signal and A.W. Thomas, Phys. Rev. **D 44** (1991) 2653;
A.W. Thomas, Phys. Lett. **B 126** (1983) 97.
- [9] H. Mineo, W. Bentz, N. Ishii and K. Yazaki, Nucl. Phys. **A 703** (2001) 785.
- [10] Y. Nambu and G. Jona-Lasinio, Phys. Rev. **122** (1960) 345; **124** (1961) 246.

- [11] T. Hatsuda and T. Kunihiro, Phys. Rep. **247** (1994) 221;
U. Vogl and W. Weise, Prog. Part. Nucl. Phys. **27** (1991) 195.
- [12] N. Ishii, W. Bentz and K. Yazaki, Phys. Lett. **B 301** (1993) 165; **318** (1993) 26;
N. Ishii, W. Bentz and K. Yazaki, Nucl. Phys. **A 578** (1995) 617.
- [13] U. Zückert, R. Alkofer, H. Weigel and H. Reinhardt, Phys. Rev. **C 55** (1997) 2030.
- [14] M. Oettel, G. Hellstern, R. Alkofer and H. Reinhardt, Phys. Rev. **C 58** (1998) 2459;
M. Oettel, R. Alkofer and L. von Smekal, Eur. Phys. J. **A 8** (2000) 553.
- [15] S. Huang and J. Tjon, Phys. Rev. **C 49** (1994) 1702;
C. Hanhart and S. Krewald, Phys. Lett. **B 344** (1995) 55;
S. Pepin, M. Birse, and J.A. McGovern, Phys. Rev. **C 61** (2000) 055209.
- [16] H. Mineo, W. Bentz and K. Yazaki, Phys. Rev. **C 60** (1999) 065201.
- [17] W. Bentz and A.W. Thomas, Nucl. Phys. **A 696** (2001) 138.
- [18] R. S. Hayano, S. Hirenzaki and A. Gillitzer, Eur. Phys. J. A **6**, 99 (1999)
- [19] K. Tsushima, D. H. Lu, A. W. Thomas and K. Saito, Phys. Lett. B **443**, 26 (1998)
- [20] K. Saito, K. Tsushima, D. H. Lu and A. W. Thomas, Phys. Rev. **C 59**, 1203 (1999)

- [21] D. Ebert, T. Feldmann and H. Reinhardt, Phys. Lett. **388** (1996) 154;
G. Hellstern, R. Alkofer and H. Reinhardt, Nucl. Phys. **A 625** (1997) 697.
- [22] Y. Nambu, Phys. Rev. **117** (1960) 648;
L.P. Gorkov, JETP **7** (1958) 993.
- [23] D. Kahana and U. Vogl, Phys. Lett. **B 244** (1990) 10;
M. Mukerjee and Y. Nambu, Ann. Phys. **191** (1989) 143.
- [24] P.A.M. Guichon, Phys. Lett. **B 200** (1988) 235;
K. Saito, K. Tsushima and A.W. Thomas, Phys. Rev. **C 55** (1997) 2637.
- [25] H. Reinhardt, Phys. Lett. **B 244** (1990) 316.
- [26] B.D. Serot and J.D. Walecka, Adv. Nucl. Phys. **11** (1986) 1.
- [27] K. Tanaka and W. Bentz, Nucl. Phys. **A 540** (1992) 383.
- [28] A. Buck, R. Alkofer and H. Reinhardt, Phys. Lett. **286** (1992) 29.
- [29] J. Boguta, Phys. Lett. **B 120** (1983) 34;
W. Bentz, L.G. Liu and A. Arima, Ann. Phys. **188** (1988) 61.
- [30] S. Ichii, W. Bentz, A. Arima and T. Suzuki, Nucl. Phys. **A 487** (1988) 493;
G.E. Brown, W. Weise, G. Baym and J. Speth, Comments Nucl. Part. Phys. **17** (1987) 39.
- [31] A.L. Fetter and J.D. Walecka, Quantum theory of many-particle systems (McGraw-Hill, New York, 1971).

- [32] I.N. Mishustin, L.M. Satarov, H. Stöcker and W. Greiner, hep-ph/0203241.
- [33] D.T. Son, Phys. Rev. **D 59** (1999) 094019.
- [34] A.W. Thomas, Adv. Nucl. Phys. **13** (1984) 1.
- [35] M.B. Hecht, M. Oettel, C.D. Roberts, S.M. Schmidt, P.C. Tandy and A.W. Thomas, Phys. Rev. **C 65** (2002) 055204.
- [36] N. Ishii, Nucl. Phys. **A 689** (2001) 793.

Appendices

A Hadronization in the path integral formalism

In this Appendix we present some formulae which are used in sect. 3.1. The Lagrangian density is given by (2.6), supplemented by (3.9).

A.1 Functional integration formulae

To derive (3.10), (3.11), the integration over the quark fields is done by using the formula

$$\int \mathcal{D}\psi \int \mathcal{D}\bar{\psi} \exp \left(i \left[\bar{\Psi} S^{-1} \Psi + \bar{\Psi} \xi + \bar{\xi} \Psi \right] \right) = \exp \left(i \left[-\frac{i}{2} \text{Tr} \ln S^{-1} + \bar{\xi} S \xi \right] \right). \quad (\text{A.1})$$

To derive (3.21), (3.22), we replace $\Delta \rightarrow \frac{\delta}{\delta(iJ^*)}$, $\Delta^* \rightarrow \frac{\delta}{\delta(iJ)}$ in the interaction part \mathcal{S}_{DI} , and use the formula

$$\int \mathcal{D}\Delta \int \mathcal{D}\Delta^* \exp \left(i \left[\Delta D^{-1} \Delta^* + \Delta^* J + J^* \Delta \right] \right) = \exp \left(i \left[i \text{Tr} \ln D^{-1} - J^* D J \right] \right). \quad (\text{A.2})$$

Finally, to derive (3.27), one integrates over the nucleon sources $\bar{\phi}$ and ϕ by using a relation analogous to (A.1), i.e.,

$$\int \mathcal{D}\phi \int \mathcal{D}\bar{\phi} \exp \left(i \left[\bar{\phi} G_N \phi + \bar{\phi} N + \bar{N} \phi \right] \right) = \exp \left(i \left[-i \text{tr} \ln G_N + \bar{N} G_N N \right] \right). \quad (\text{A.3})$$

Note that the trace symbol Tr in (A.1) includes a trace in Nambu-Gorkov space, in contrast to the trace in (A.3), and therefore there is no factor $\frac{1}{2}$ in the exponent of (A.3).

A.2 Derivation of Eq.(3.18)

The first term in (3.11) involves the propagator S , which is obtained by inverting (3.12). If we write

$$S = \begin{pmatrix} S_{11} & S_{12} \\ S_{21} & S_{22} \end{pmatrix} \quad (\text{A.4})$$

then the diagonal elements are obtained as

$$S_{11} = \frac{S_0}{1 + G_0 \gamma_5 \Delta_a \beta_a \tilde{S}_0 \gamma_5 \Delta_a^* \beta_a}, \quad S_{22} = \frac{\tilde{S}_0}{1 + \tilde{S}_0 \gamma_5 \Delta_a^* \beta_a S_0 \gamma_5 \Delta_a \beta_a},$$

while the non-diagonal elements are

$$S_{12} = i S_{11} \gamma_5 \Delta_a \beta_a \tilde{S}_0, \quad S_{21} = i S_{22} \gamma_5 \Delta_a^* \beta_a S_0.$$

The quantities S_0 and \tilde{S}_0 are given in momentum space by (3.17). When the above form for S is inserted into (3.11), the non-diagonal elements of S lead to terms which involve different numbers of Δ or Δ^* , and these terms vanish after the integration over the diquark fields. Therefore the first term in (3.11) effectively becomes

$$\frac{1}{3} \overline{\Phi} \begin{pmatrix} \Delta S_{11} \Delta^* & 0 \\ 0 & \Delta^* S_{22} \Delta \end{pmatrix} \Phi. \quad (\text{A.5})$$

Then one uses the Nambu-Gorkov forms of $\overline{\Phi}$ and Φ , which are expressed similar to Eq.(2.1) in terms of $\overline{\phi}$ and ϕ , and the relations $C \tilde{S}_0^T C^{-1} = S_0$, $C S_0^T C^{-1} = \tilde{S}_0$, where the symbol T (transpose) stands also w.r.t. the functional matrix structure, i.e., it implies $x \leftrightarrow x'$. In this way one arrives at Eq.(3.18).

A.3 Derivation of Eq. (3.23)

Let us extract the term $\propto \bar{\phi}\phi$ from (3.21) and (3.22). The second exponential factor in (3.21) gives

$$\exp\left(-\text{Tr} \ln \left[1 + \frac{1}{3} D_0 \bar{\phi} S_0 \phi\right]\right) \quad (\text{A.6})$$

$$= 1 - \bar{\phi} (S_0 D_0) \phi + \dots \equiv 1 + i \bar{\phi} \Pi_N \phi + \dots, \quad (\text{A.7})$$

where a color factor 3 comes from the color trace in (A.6), and $\Pi_N \equiv i S_0 D_0$ as in (3.25). Next, the factor in (3.22) gives to $\mathcal{O}(\bar{\phi}\phi)$

$$\begin{aligned} & \left[\exp\left(i \mathcal{S}_{DI}(\hat{\Delta}, \hat{\Delta}^*)\right) \exp(-i J^* D J) \right]_{J=J^*=0} \\ &= 1 + i \left[\mathcal{S}_{DI}(\hat{\Delta}, \hat{\Delta}^*) \exp(-i J^* D_0 J) \right]_{J=J^*=0} + \dots \end{aligned} \quad (\text{A.8})$$

$$\begin{aligned} &= 1 + \frac{i}{3} \bar{\phi} \left\{ \left[\hat{\Delta} S_0 \frac{1}{M} (\hat{\Delta}_{a'} \beta_{a'}) (\hat{\Delta}_a^* \beta_a) S_0 \hat{\Delta}^* \right. \right. \\ & \quad \left. \left. + \hat{\Delta} S_0 \frac{1}{M} (\hat{\Delta}_{a'} \beta_{a'}) (\hat{\Delta}_a^* \beta_a) \frac{1}{M} S_0 (\hat{\Delta}_{a'} \beta_{a'}) (\hat{\Delta}_a^* \beta_a) S_0 \hat{\Delta}^* + \dots \right] \phi \right. \\ & \quad \left. \times \exp(-i J^* D_0 J) \right\}_{J=J^*=0} + \dots, \end{aligned} \quad (\text{A.9})$$

where $\hat{\Delta} \equiv \frac{\delta}{\delta(iJ^*)}$, $\hat{\Delta}^* \equiv \frac{\delta}{\delta(iJ)}$. A contraction is obtained if one $\hat{\Delta}$ and one $\hat{\Delta}^*$ hit the same factor $(-i J^* D_0 J) = (i J^*)(i D_0)(i J)$, which appears in the expansion of the exponent in (A.9). This contraction of $\hat{\Delta}_a$ with $\hat{\Delta}_{a'}$ gives a factor $i D_0 \delta_{a'a}$. Among the many contractions which emerge in (A.9), the ladder graphs appear as a subset besides self interaction graphs [13]. To obtain the ladder graphs from (A.9), one contracts $\hat{\Delta}$ on the most left side with $\hat{\Delta}^*$ to the nearest to the right of it, then the next $\hat{\Delta}$ on the left side with $\hat{\Delta}^*$ nearest to the right of it, etc. To write down the resulting series, we make the color structure more explicit by decomposing

$$\left[(\hat{\Delta}_{a'} \beta_{a'}) (\hat{\Delta}_a^* \beta_a) \right]_{kl} \equiv C_{kl}^{ab} \hat{\Delta}_a^* \hat{\Delta}_b^* = \left(-3 P_{kl}^{(0)ab} + \frac{3}{2} P_{kl}^{(8)ab} \right) \hat{\Delta}_a^* \hat{\Delta}_b^*,$$

where the color singlet and octet projection operators are given by:

$$P_{kl}^{(0)ab} = \frac{1}{3}\delta_{ka}\delta_{lb} \quad P_{kl}^{(8)ab} = \delta_{kl}\delta_{ab} - \frac{1}{3}\delta_{ka}\delta_{lb}$$

Then the ladder-type contribution from (A.9) is given by

$$\begin{aligned} 1 &+ \frac{i\bar{\phi}}{3} \left[\Pi_N \frac{1}{M} \Pi_N C_{ij}^{ij} + \Pi_N \frac{1}{M} \Pi_N \frac{1}{M} \Pi_N C_{ib}^{ib} C_{lj}^{bj} + \dots \right] \phi \\ &= 1 + i\bar{\phi} \Pi_N T_N \Pi_N \phi \end{aligned} \quad (\text{A.10})$$

where the quark-diquark T-matrix is given in (3.26). The sum of (A.7) and (A.10) is then $1 + i\bar{\phi}G_N\phi = \exp(i\bar{\phi}G_N\phi) + \dots$, where the quark-diquark propagator in the color singlet channel, G_N , is given by (3.24). In this way one arrives at (3.23).

B Explicit evaluation of the Dirac determinant

The contribution of the quark loop to the effective action is (see Eq.(3.38)) $-\frac{i}{2}\text{Tr} \ln S^{-1} \equiv -\int d^4x V_\ell$, where the inverse quark propagator is a 2×2 matrix in Nambu-Gorkov space and given by (3.36). By using the relation

$$\text{Tr} \ln \begin{pmatrix} A & B \\ C & D \end{pmatrix} = \text{Tr} \ln (-B C + B D B^{-1} A)$$

and $\beta_1^2 = \frac{3}{2}\text{diag}(0, 1, 1) \equiv \frac{3}{2}C_1$, we obtain

$$V_\ell = \frac{i}{2} \int \frac{d^4p}{(2\pi)^4} \text{Tr} \ln \left(\Delta^2 C_1 + (-\not{p} - M + \nu\gamma_0)(\not{p} - M + \nu\gamma_0) \right), \quad (\text{B.1})$$

where we defined $\nu \equiv \mu_q^*$ to simplify the notation. For the evaluation of the Dirac determinant it is sufficient, because of rotational invariance, to consider

the vector \mathbf{p} along the z-axis, and (B.1) becomes

$$V_\ell = \frac{i}{2} \int \frac{d^4 p}{(2\pi)^4} \text{Tr} \ln \left(\Delta^2 C_1 - p_0^2 + p^2 + M^2 + \nu^2 - 2M\nu\gamma^0 + 2\nu p\gamma^3\gamma^0 \right),$$

where in this Appendix we use the notation $p^2 \equiv \mathbf{p}^2$ and $E_p \equiv \sqrt{p^2 + M^2}$. By using explicit representations for the Dirac matrices, it is easy to calculate the Dirac determinant explicitly. Because of isospin we get a factor 2, and one is left only with the color determinant:

$$V_\ell = 2i \int \frac{d^4 p}{(2\pi)^4} \ln \det_C \left[\left(\Delta^2 C_1 - p_0^2 + E_p^2 + \nu^2 \right)^2 - 4E_p^2 \nu^2 \right]. \quad (\text{B.2})$$

By using $C_1 = \text{diag}(0, 1, 1)$, one can calculate the color determinant with the result

$$V_\ell = 2i \int \frac{d^4 p}{(2\pi)^4} \left\{ 2 \ln \left[(p_0^2 - \epsilon_+^2) (p_0^2 - \epsilon_-^2) \right] + \ln \left[(p_0^2 - \epsilon_{0+}^2) (p_0^2 - \epsilon_{0-}^2) \right] \right\}, \quad (\text{B.3})$$

where $\epsilon_\pm^2 = (E_p \pm \nu)^2 + \Delta^2$ and $\epsilon_{0\pm}^2 = (E_p \pm \nu)^2$. In this way one arrives at (3.38).

It is convenient to separate the part which survives for $\Delta = 0$ from the rest. The latter contribution to the effective potential is given by the first line of (3.41). The former contribution becomes, after subtracting the zero density value,

$$V_\ell(\Delta = 0) = 6i \int \frac{d^4 p}{(2\pi)^4} \left[\ln \frac{p_0^2 - (E_p + \nu)^2}{p_0^2 - E_{0p}^2} + \ln \frac{p_0^2 - (E_p - \nu)^2}{p_0^2 - E_{0p}^2} \right], \quad (\text{B.4})$$

where $E_{0p} = \sqrt{M_0^2 + p^2}$. This can further be split into the pure vacuum loop which contributes to V_{vac} given in (3.34), and the density dependent term

$$V_Q = 6i \int \frac{d^4 p}{(2\pi)^4} \left[\ln \frac{p_0^2 - (E_p + \nu)^2}{p_0^2 - E_p^2} + \ln \frac{p_0^2 - (E_p - \nu)^2}{p_0^2 - E_p^2} \right]$$

$$\begin{aligned}
&= -6 \int \frac{d^3 p}{(2\pi)^3} [(E_p + \nu) - E_p + |E_p - \nu| - E_p] \\
&= -12 \int \frac{d^3 p}{(2\pi)^3} \Theta(\nu - E_p) (\nu - E_p), \tag{B.5}
\end{aligned}$$

which is Eq.(3.40).

We also note that the evaluation of the nucleonic contribution, (3.30), to the effective potential for NM proceeds similarly, by setting $\Delta = 0$ in (B.1) and replacing $M \rightarrow M_N$, $\nu \rightarrow \mu^*$. (Of course, there is no color factor 3 in this case.) Since the contribution for $\mu = 0$ is subtracted, one is left with the density dependent piece (3.32).

C The ω meson in nuclear and quark matter

The expression for the the $q\bar{q}$ bubble graph in quark matter (Fermi momentum p_F) for an external isoscalar vector field with $q^\mu = (q^0, \mathbf{0})$ is given by

$$\Pi^{\mu\nu}(q) = \int \frac{d^4 k}{(2\pi)^4} \Theta(|\mathbf{k}| - p_F) \text{Tr} \frac{\gamma^\mu (\not{k} + M) \gamma^\nu (\not{k} + \not{q} + M)}{(k^2 - M^2) ((k + q)^2 - M^2)}. \tag{C.1}$$

We introduce a Feynman parameter (x) and make a shift $k \rightarrow k - qx$. Since $\mathbf{q} = 0$, this shift affects only the time component, which is no problem since the proper time regularization scheme does not directly cut the loop momentum. The evaluation of the Dirac trace gives a term $\propto k^\mu k^\nu$, for which we perform a partial integration, thereby picking up a surface term arising from the Θ function in (C.1). The result is $\Pi^{00}(q) = 0$ and $\Pi^{ij}(q) \equiv g^{ij} \Pi(q)$ with

$$\Pi(q) = -48 q_0^2 \int \frac{d^4 k}{(2\pi)^4} \Theta(|\mathbf{k}| - p_F) \int_0^1 dx \frac{x(1-x)}{(k^2 + M^2 - q_0^2 x(1-x))^2} \tag{C.2}$$

$$+ 8p_F \int \frac{d^4k}{(2\pi)^4} \delta(|\mathbf{k}| - p_F) \int_0^1 dx \frac{1}{k^2 + M^2 - q_0^2 x(1-x)} \quad (\text{C.3})$$

Here we performed a Wick rotation in k_0 . This expression is now regularized according to the prescription (4.42). (In order that the imaginary part is canceled for the case $\Lambda_{\text{IR}} > 0$, the finite surface term (C.3) has to be treated in the same way as the divergent part (C.2).) For the part (C.2) we introduce Euclidean polar coordinates (k, Θ) by $|\mathbf{k}| = k \sin \Theta$, $k_0 = k \cos \Theta$, where Θ is restricted by $0 \leq \Theta \leq \arcsin \frac{p_F}{k}$. After performing the Θ integration we obtain for the piece (C.2), which we call $\hat{\Pi}$,

$$\begin{aligned} \hat{\Pi}(q) &= -\frac{3}{\pi^2} q_0^2 \int_{p_F^2}^{\infty} t dt G \left(\sqrt{\frac{p_F^2}{t}} \right) \int_0^1 dx x(1-x) \int_{1/\Lambda_{\text{UV}}^2}^{1/\Lambda_{\text{IR}}^2} d\tau \tau \\ &\times \exp \left(-\tau \left[t + M^2 - q_0^2 x(1-x) \right] \right), \end{aligned} \quad (\text{C.4})$$

where

$$G(y) = 1 - \frac{2}{\pi} \left(\arcsin y - y \sqrt{1-y^2} \right).$$

The τ integration can also be performed, and the final result is

$$\begin{aligned} \hat{\Pi}(q) &= -\frac{3}{\pi^2} q_0^2 \int_{p_F^2}^{\infty} t dt G \left(\sqrt{\frac{p_F^2}{t}} \right) \int_0^1 dx x(1-x) \frac{1}{A^2} \\ &\times \left[e^{-A/\Lambda_{\text{UV}}^2} \left(1 + \frac{A}{\Lambda_{\text{UV}}^2} \right) - e^{-A/\Lambda_{\text{IR}}^2} \left(1 + \frac{A}{\Lambda_{\text{IR}}^2} \right) \right], \end{aligned} \quad (\text{C.5})$$

where $A = t + M^2 - q_0^2 x(1-x)$. For $\Lambda_{\text{IR}} > 0$, [...] in (C.5) behaves $\propto A^2$ for $A \rightarrow 0$, and there is no imaginary part. The piece (C.3) is given by

$$\delta\Pi(q) = \frac{4p_F^3}{\pi^3} \int_0^{\infty} dk_0 \int_0^1 dx \frac{\exp(-B/\Lambda_{\text{UV}}^2) - \exp(-B/\Lambda_{\text{IR}}^2)}{B},$$

where $B = k_0^2 + M^2 + p_F^2 - q_0^2 x(1-x)$.

D Numerical results for other choices of parameters

In this Appendix we present some numerical results for the QM EOS obtained by using values of Λ_{IR} or r_ω other than those used in the main text.

First we consider the case where the same strength of the vector interaction as in NM ($r_\omega = 0.37$) is used also in QM, taking $\Lambda_{\text{IR}} = 0$ in QM. The results are shown in Fig. 15. The dotted line here ($r_s = 0$ in QM) is very similar to the dashed line for $r_\omega = 0.37$ in Fig. 5. (We note that in Fig. 5 we used $\Lambda_{\text{IR}} = 0.2$ GeV.) It is clear from Fig. 15 that it is not possible to have a NM \rightarrow QM phase transition, even if one uses large values of r_s .

Next we consider the case where the same value of the IR cut-off as in NM ($\Lambda_{\text{IR}} = 0.2$ GeV) is used also in QM, taking $r_\omega = 0$ in QM. The results are shown in Fig. 16. The dotted line here ($r_s = 0$ in QM) agrees with the dashed line for $r_\omega = 0$ in Fig. 5. We see that the qualitative behavior of the curves with increasing r_s is similar to the case $\Lambda_{\text{IR}} = 0$ shown in Fig. 8, although the sensitivity to the pairing strength r_s is somewhat stronger for the case $\Lambda_{\text{IR}} = 0$. (For given r_s , the gaps are larger for the case of $\Lambda_{\text{IR}} = 0$.) The case of $r_s = 0.25$, shown in Fig. 16, is actually very similar to the case $r_s = 0.2$ in Fig. 8, which was used in sect. 4.3 as an example to illustrate the NM \rightarrow QM phase transition.

Tables

	Nucleons and NM	QM
m [MeV]	16.93	17.08
G_π [GeV ⁻²]	19.60	19.76
Λ_{UV} [MeV]	638.5	636.7
Λ_{IR} [MeV]	200.0	0
r_ω	0.37	0
r_s	0.51	free parameter

Table 1: Parameters used for single nucleons, nuclear matter (left column) and quark matter (right column). The proper time regularization scheme is used in both cases.

Figure Captions

1. Nucleon mass as function of scalar potential for $\Lambda_{\text{IR}} = 0.2 \text{ GeV}$ and $\Lambda_{\text{IR}} = 0$. The parameter set for $\Lambda_{\text{IR}} = 0.2 \text{ GeV}$ is shown in Table 1, and that for $\Lambda_{\text{IR}} = 0$ can be found in Table 1 of Ref.[17]. The quark-diquark threshold for the case $\Lambda_{\text{IR}} = 0$ is also shown.
2. Binding energy per nucleon as function of density for $\Lambda_{\text{IR}} = 0.2 \text{ GeV}$ and $\Lambda_{\text{IR}} = 0$. The parameter set for $\Lambda_{\text{IR}} = 0.2 \text{ GeV}$ is shown in Table 1, while that for $\Lambda_{\text{IR}} = 0$ can be found in Table 1 of Ref.[17].
3. The nucleon and quark effective masses in NM (solid lines), and the quark effective mass in normal (non-superconducting) QM (dashed line) are shown as functions of the density. The parameters used in the NM calculation are shown in the second row of Table 1, and the result for QM shown here refers to the same parameter set. (Note that the parameters r_ω and r_s are relevant only for the NM result shown in this figure.)
4. Effective mass of the ω meson at rest ($\mathbf{q} = 0$) in NM as function of the density. The dashed line shows the density dependence of $2M^*$. The parameters used in the calculation are shown in the second row of Table 1.
5. $P-\mu$ plots for NM (solid line and insert) and normal (non-superconducting) QM. The two dashed lines show the QM result for two values of r_ω , and the dotted lines show the massless quark gas EOS for two values of the bag constant B . The parameters used in the NM calculation are shown in the second row of Table 1, and the results for QM

shown here refer to the same parameter set, apart from the variation of the parameter r_ω . (Both dashed lines in this figure start at the point $(\mu, P) = (1200 \text{ MeV}, 0)$, corresponding to zero density. For the case $r_\omega = 0.37$ the pressure increases monotonously, while for $r_\omega = 0$ the pressure first increases slightly for very small densities, then decreases to negative values (unstable branch), and finally increases.)

6. Effective mass of the ω meson at rest ($\mathbf{q} = 0$) in QM, as function of the density, for the case $\Lambda_{\text{IR}} = 0.2 \text{ GeV}$. The variation of the effective quark mass with density used in this calculation is shown by the dashed line in Fig. 3. The values of r_ω used in the calculation of the effective ω -meson mass are indicated for each line. The dashed line shows the density dependence of $2\sqrt{M^{*2} + p_F^2}$.
7. Same as Fig. 6 for the case $\Lambda_{\text{IR}} = 0$. For small r_ω , solutions exist only in the high density region.
8. $P - \mu$ plots for NM (solid line) and QM for several values of the pairing strength r_s in QM. The parameters used in the calculation are shown in the second and third rows of Table 1, and the values of r_s in QM are indicated in the figure. A crossing of the NM and QM lines indicates a first order phase transition. The dotted line ($r_s = 0$) differs slightly from the result shown in Figure 5 for $r_\omega = 0$, since for Fig. 5 the parameters shown in the second row of Table 1 were also used in the QM calculation.
9. The effective quark masses in NM (solid line) and QM for several values of the pairing strength r_s in QM as functions of the density. The cases

1 to 6 indicated in this figure refer to different choices of r_s in QM as indicated in Fig. 8. The dotted line ($r_s = 0$) differs from the result shown in Fig. 3, since for Fig. 3 the parameters shown in the second row of Table 1 were also used in the QM calculation.

10. The gap in QM for several values of the pairing strength, r_s , as a function of the density. The cases 1 to 6 indicated in this figure refer to the different choices of r_s shown in Fig. 8.
11. The density of the ground state as function of the chemical potential. The ground state of the system is either the vacuum (VAC), nuclear matter (NM) or superconducting quark matter (QM). The pairing strength $r_s = 0.2$ is used for QM.
12. The quark effective masses (solid lines) and the gap (dashed line) of the ground state as functions of the chemical potential. The ground state of the system is either the vacuum (VAC), nuclear matter (NM) or superconducting quark matter (QM). The value of the gap is equal to zero for VAC and NM. The pairing strength $r_s = 0.2$ is used for QM.
13. The pressure in the ground state as function of the density. The ground state of the system is either the vacuum (VAC), nuclear matter (NM) or superconducting quark matter (QM). (The vacuum corresponds to the point $P = 0$, $\rho = 0$.) The dashed lines indicate the mixed phases. The pairing strength $r_s = 0.2$ is used for QM.
14. The energy density of the ground state as function of the density. The ground state of the system is either the vacuum (VAC), nuclear matter (NM) or superconducting quark matter (QM). (The vacuum corre-

sponds to the point $\mathcal{E} = 0, \rho = 0$.) The dashed lines indicate the mixed phases. The pairing strength $r_s = 0.2$ is used for QM.

15. $P - \mu$ plots for NM (solid line) and QM for several values of the pairing strength, r_s , in QM. The case shown here refers to $\Lambda_{\text{IR}} = 0$ and $r_\omega = 0.37$ in QM.
16. $P - \mu$ plots for NM (solid line) and QM for several values of the pairing strength, r_s , in QM. The case shown here refers to $\Lambda_{\text{IR}} = 0.2 \text{ GeV}$ and $r_\omega = 0$ in QM.

Figure 1

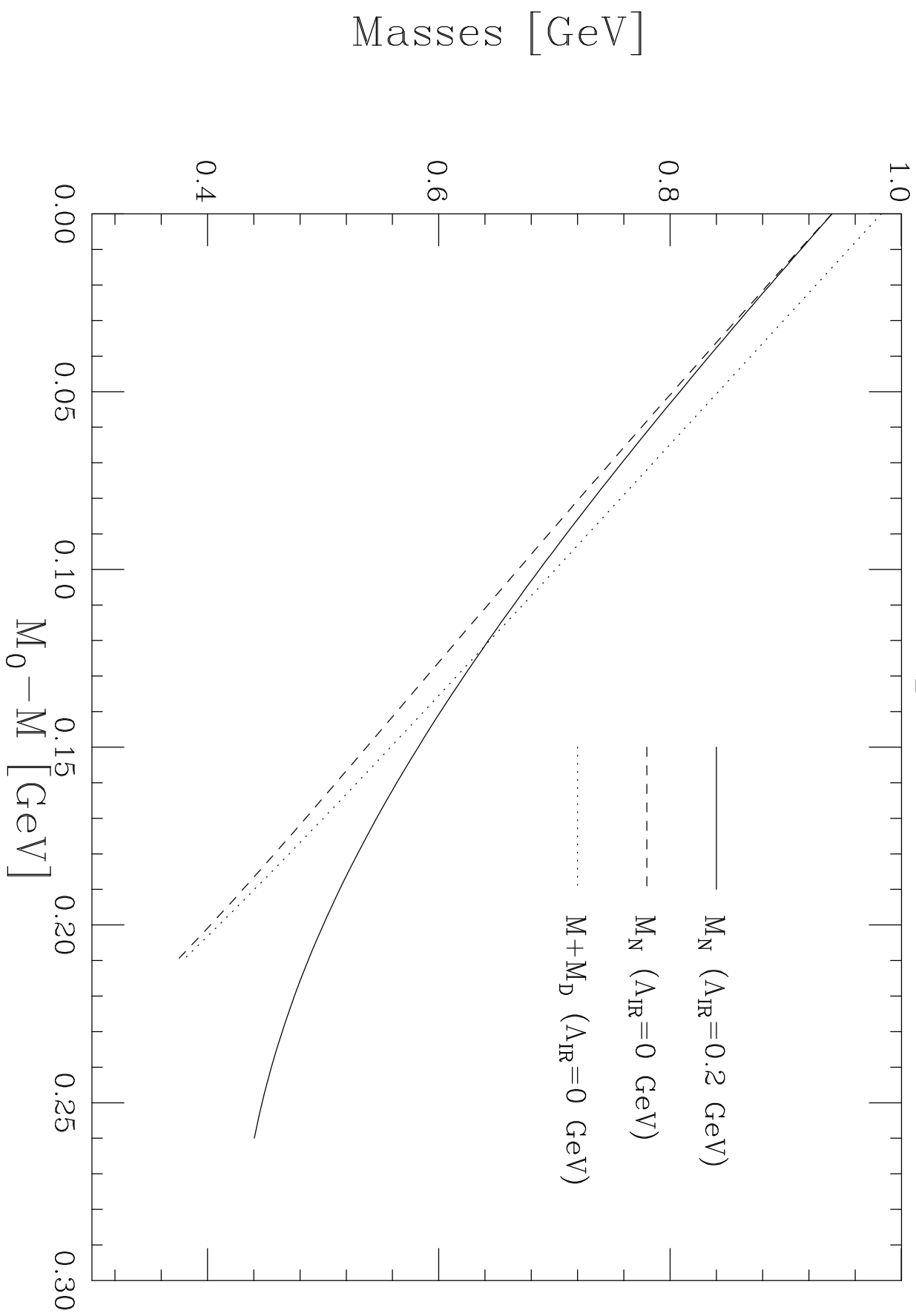


Figure 2

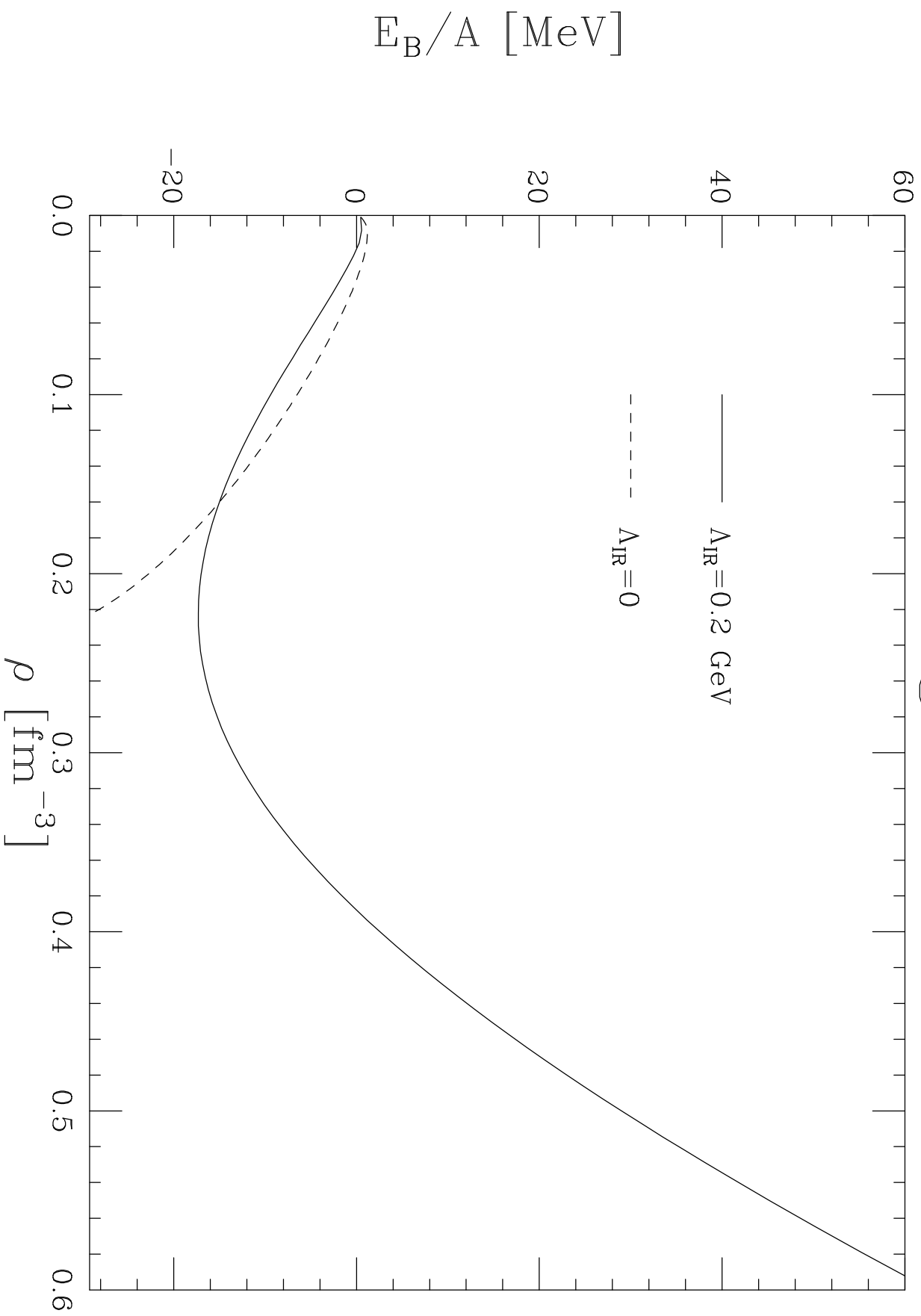


Figure 3

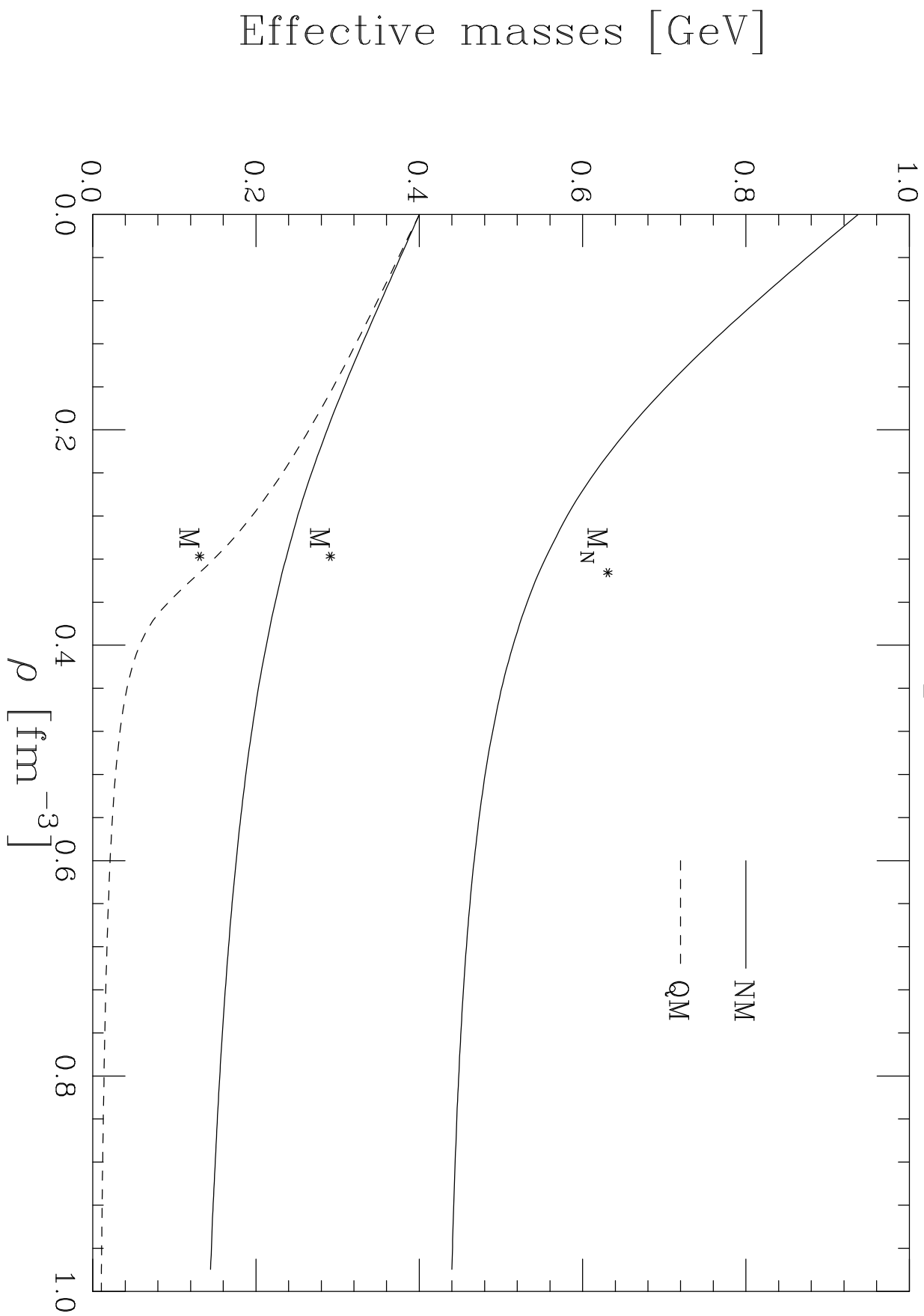


Figure 4

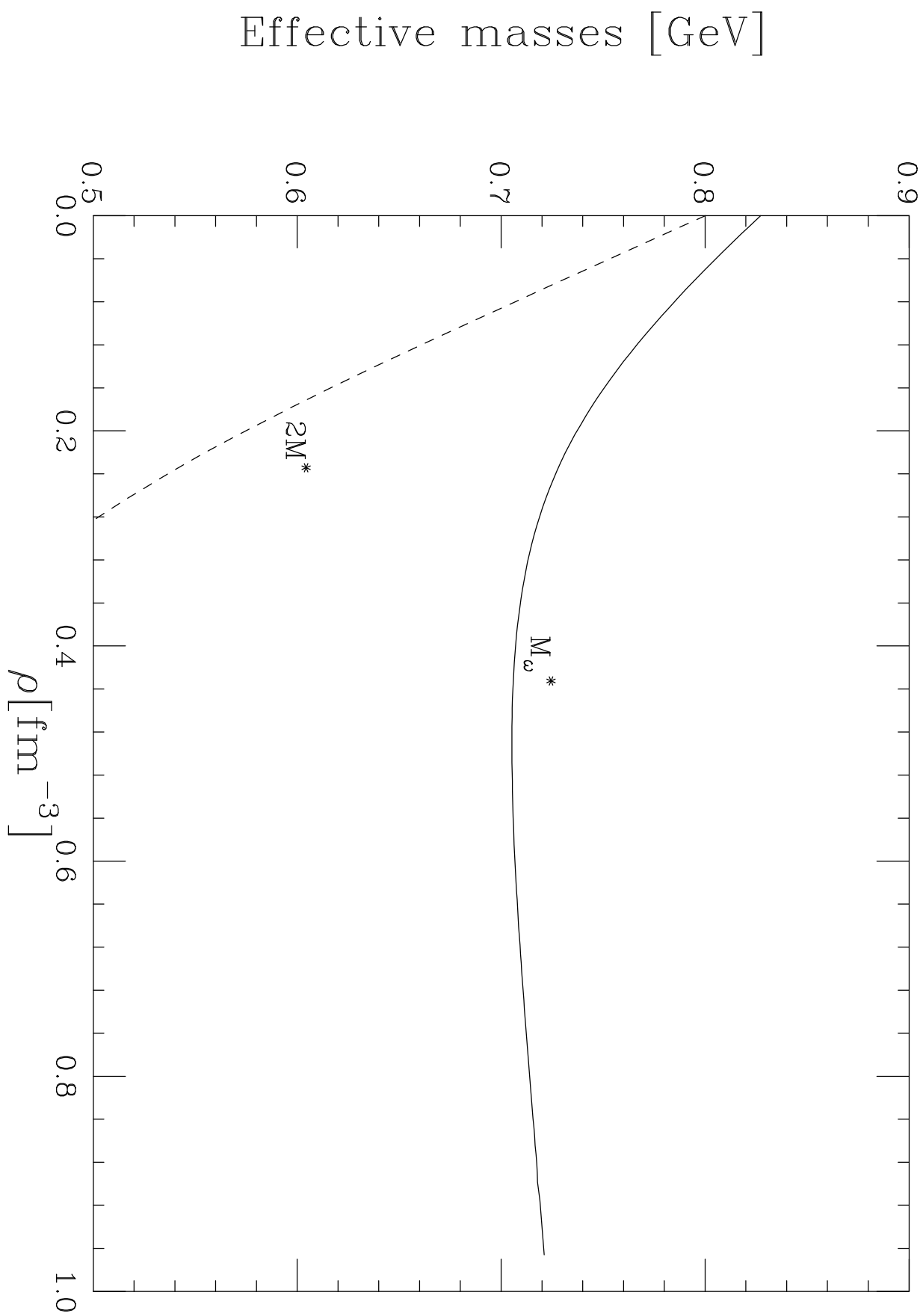


Figure 5

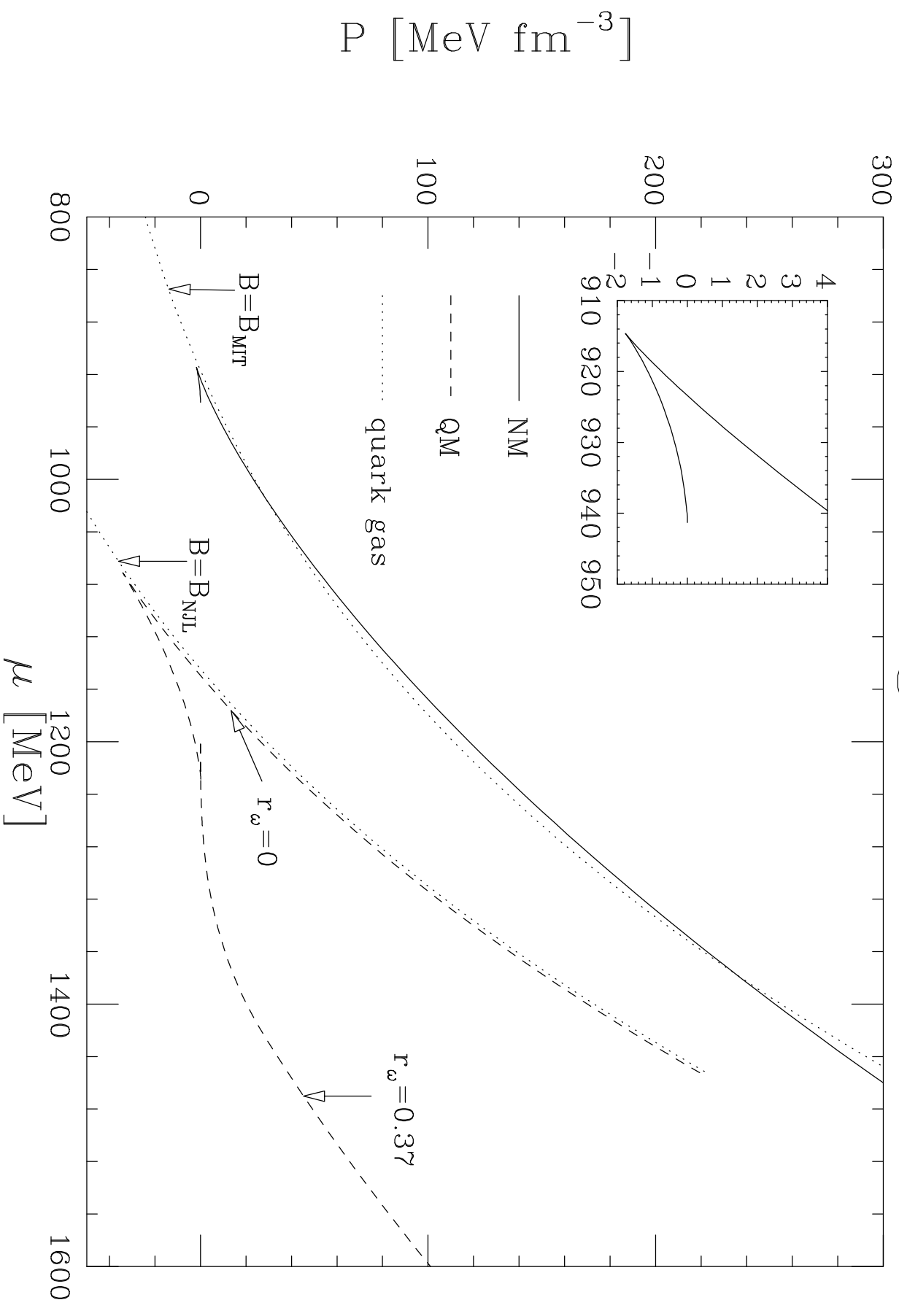


Figure 6

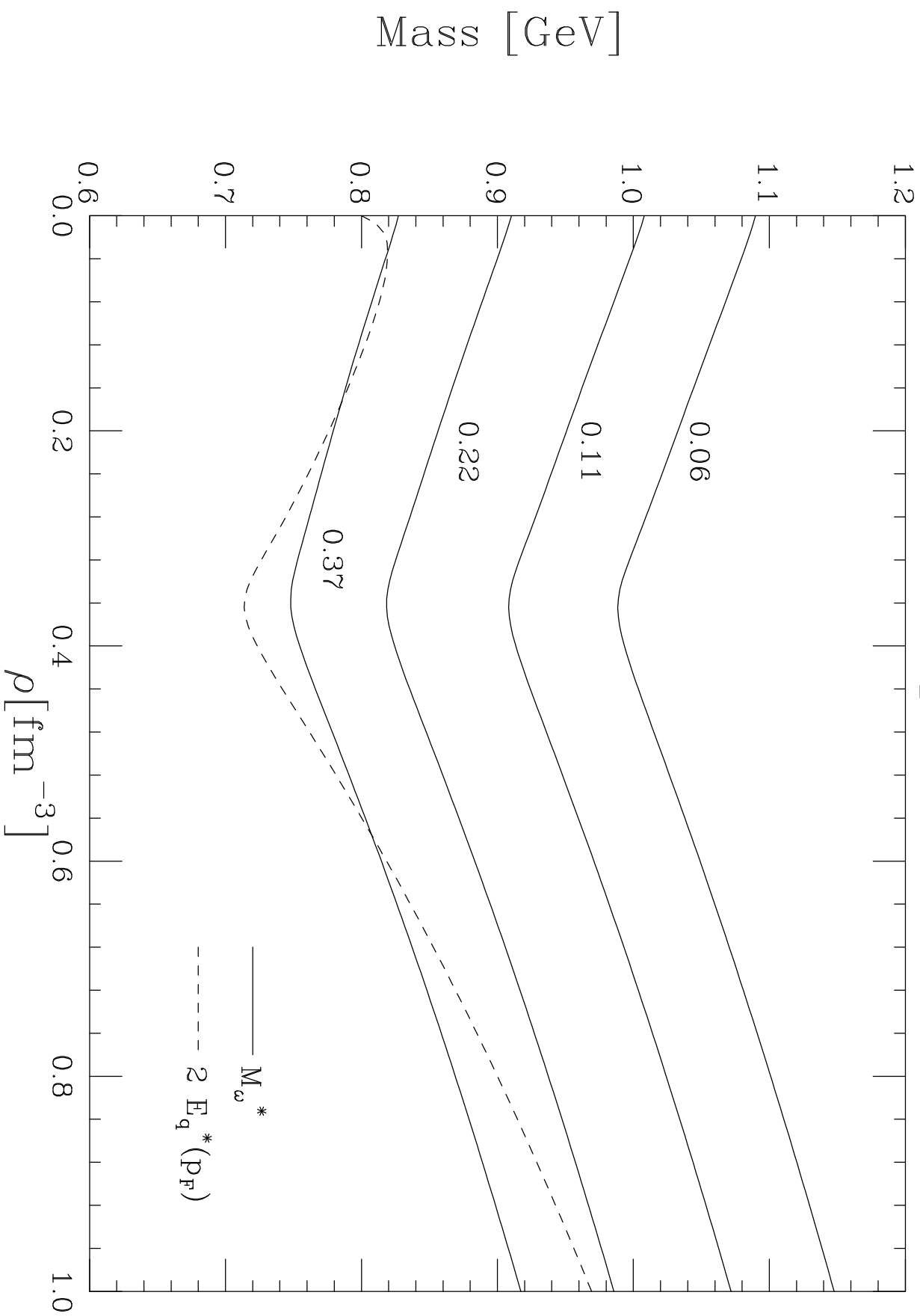


Figure 7

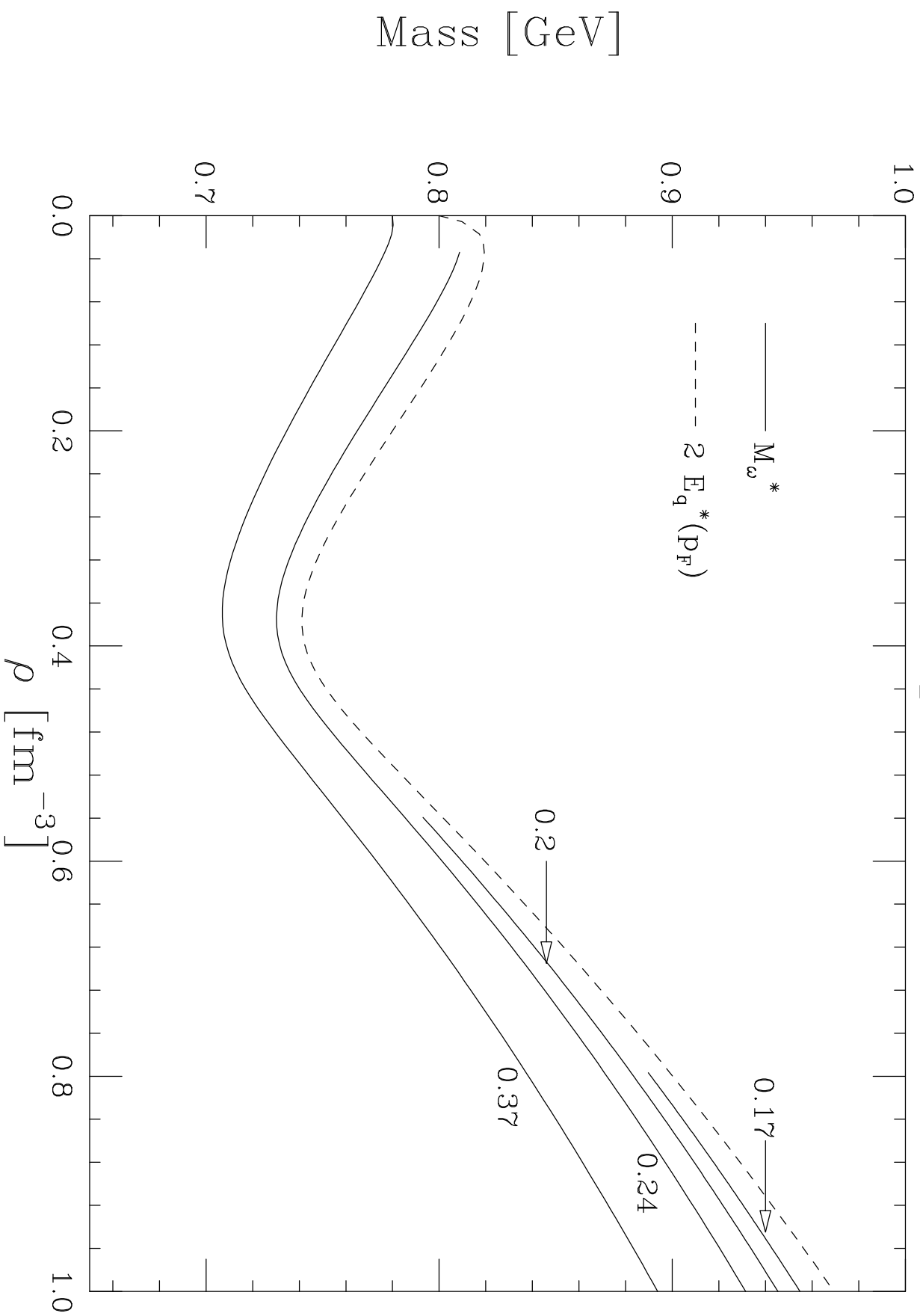


Figure 8

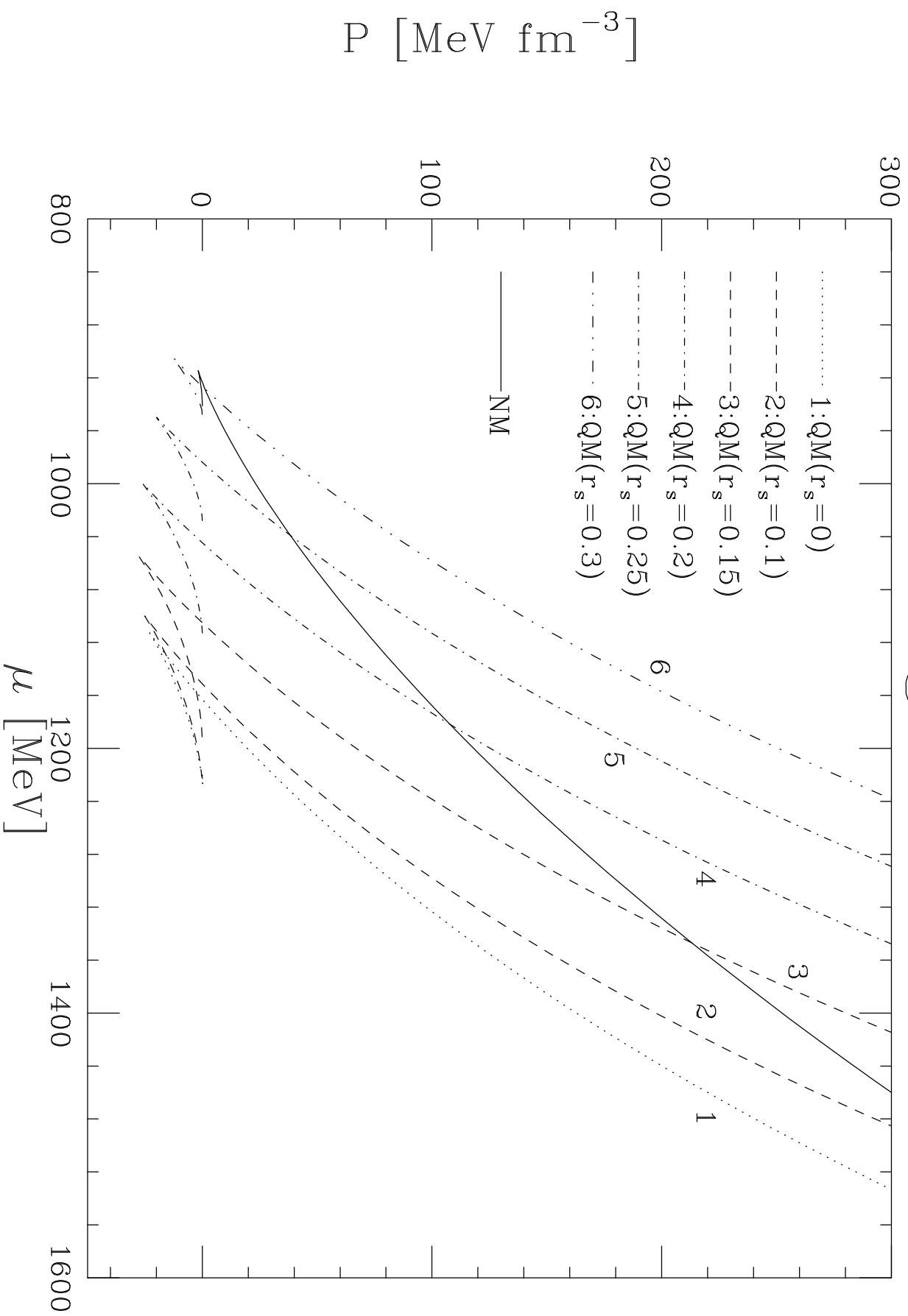


Figure 9

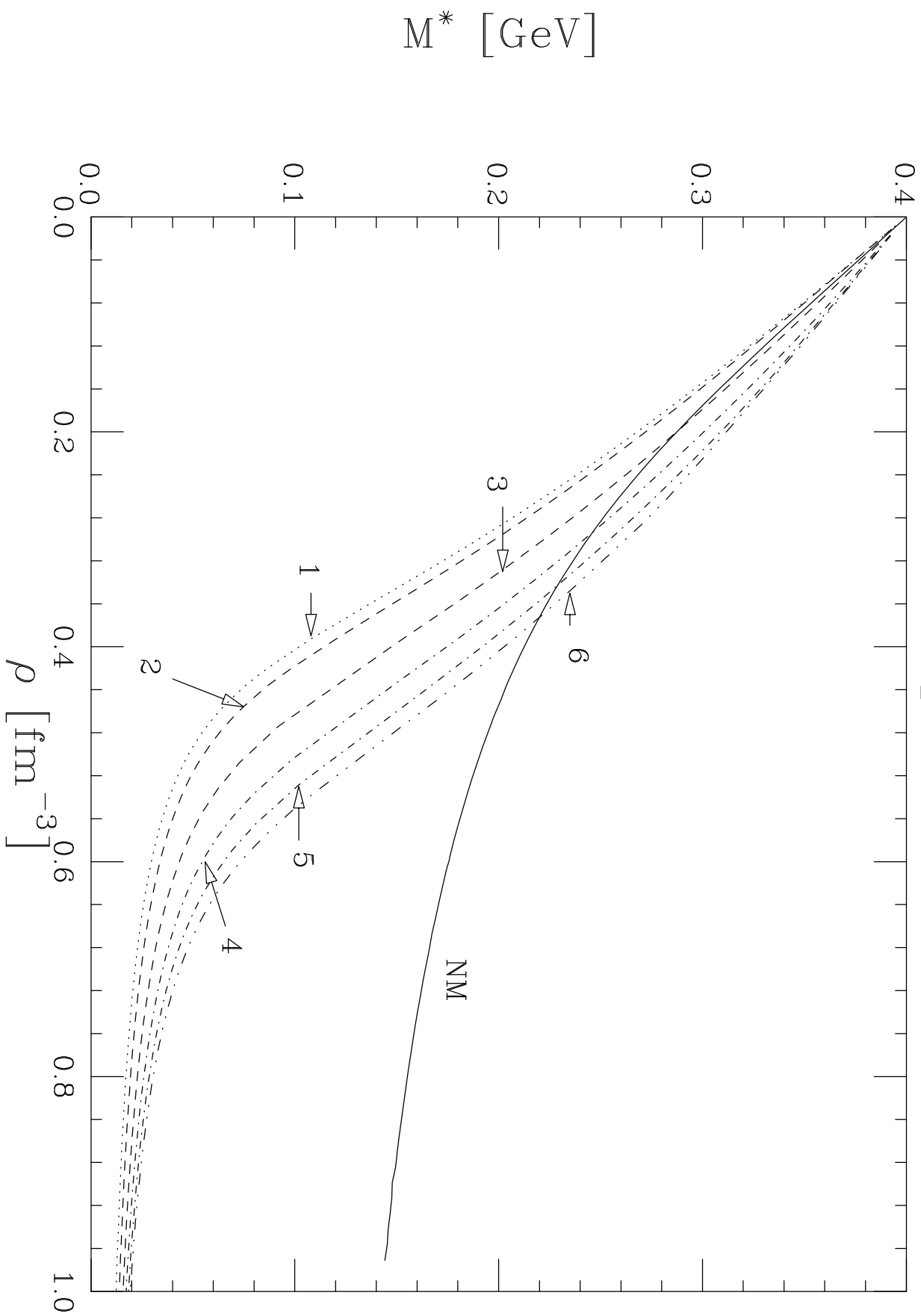


Figure 10

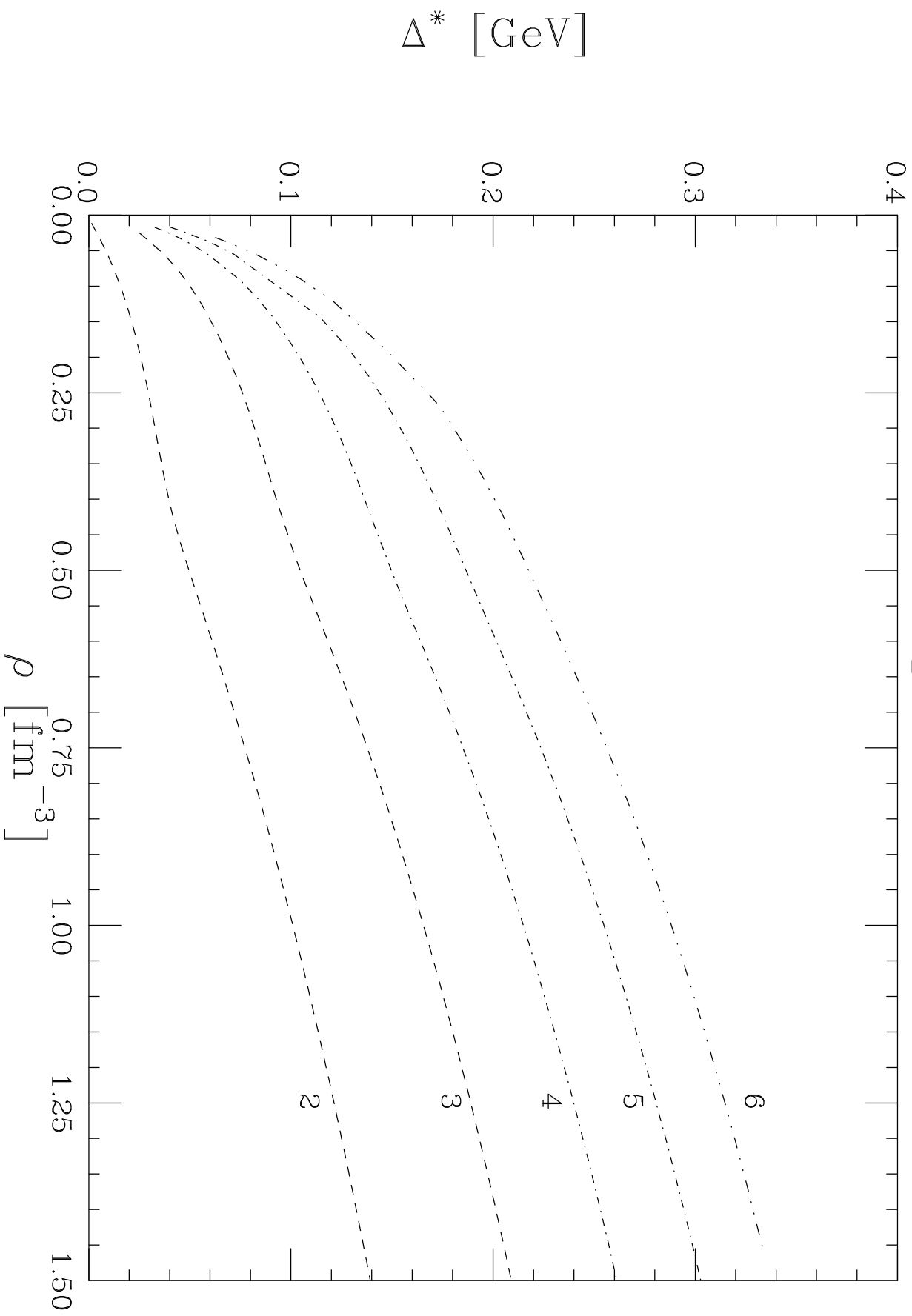


Figure 11

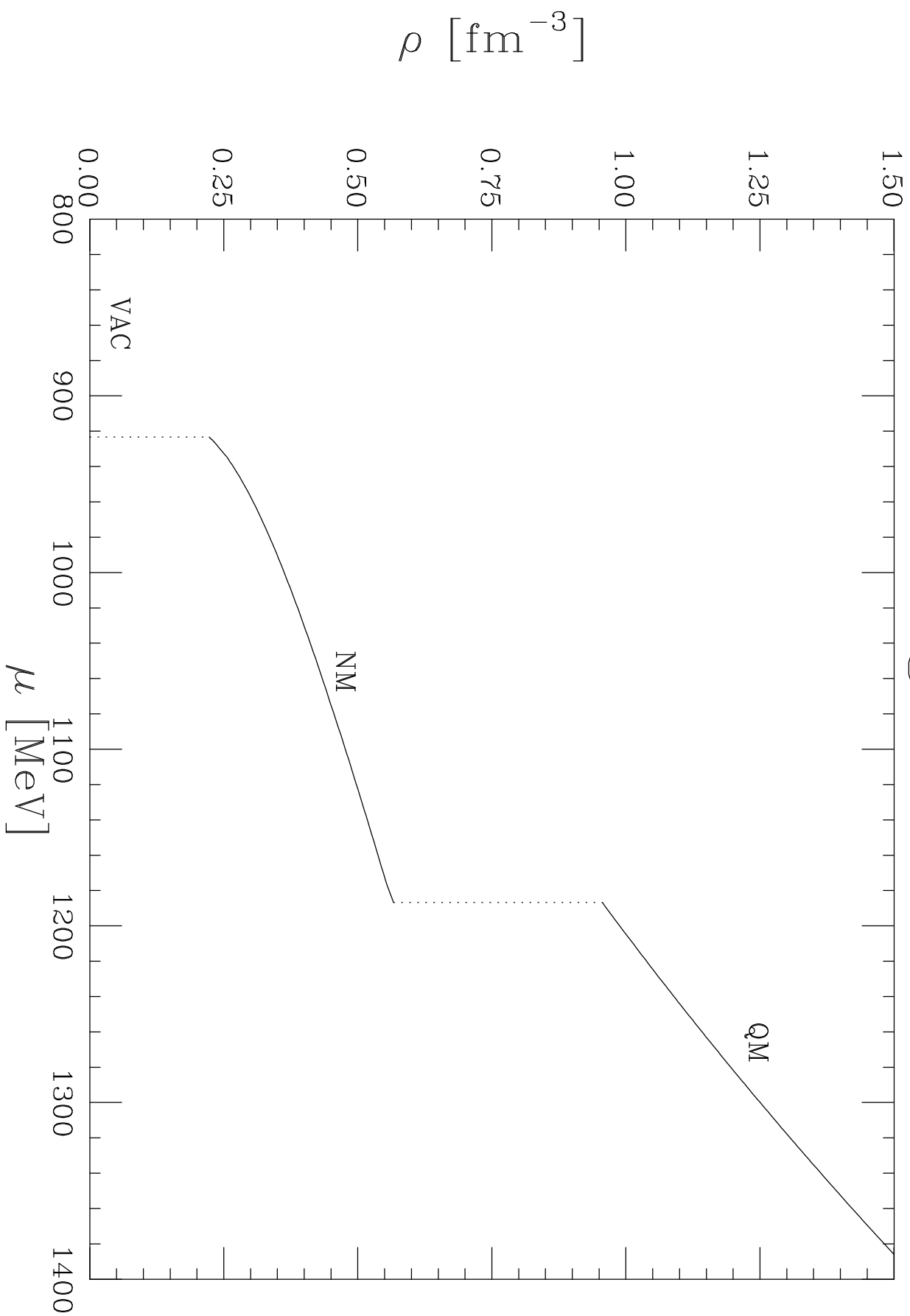


Figure 12

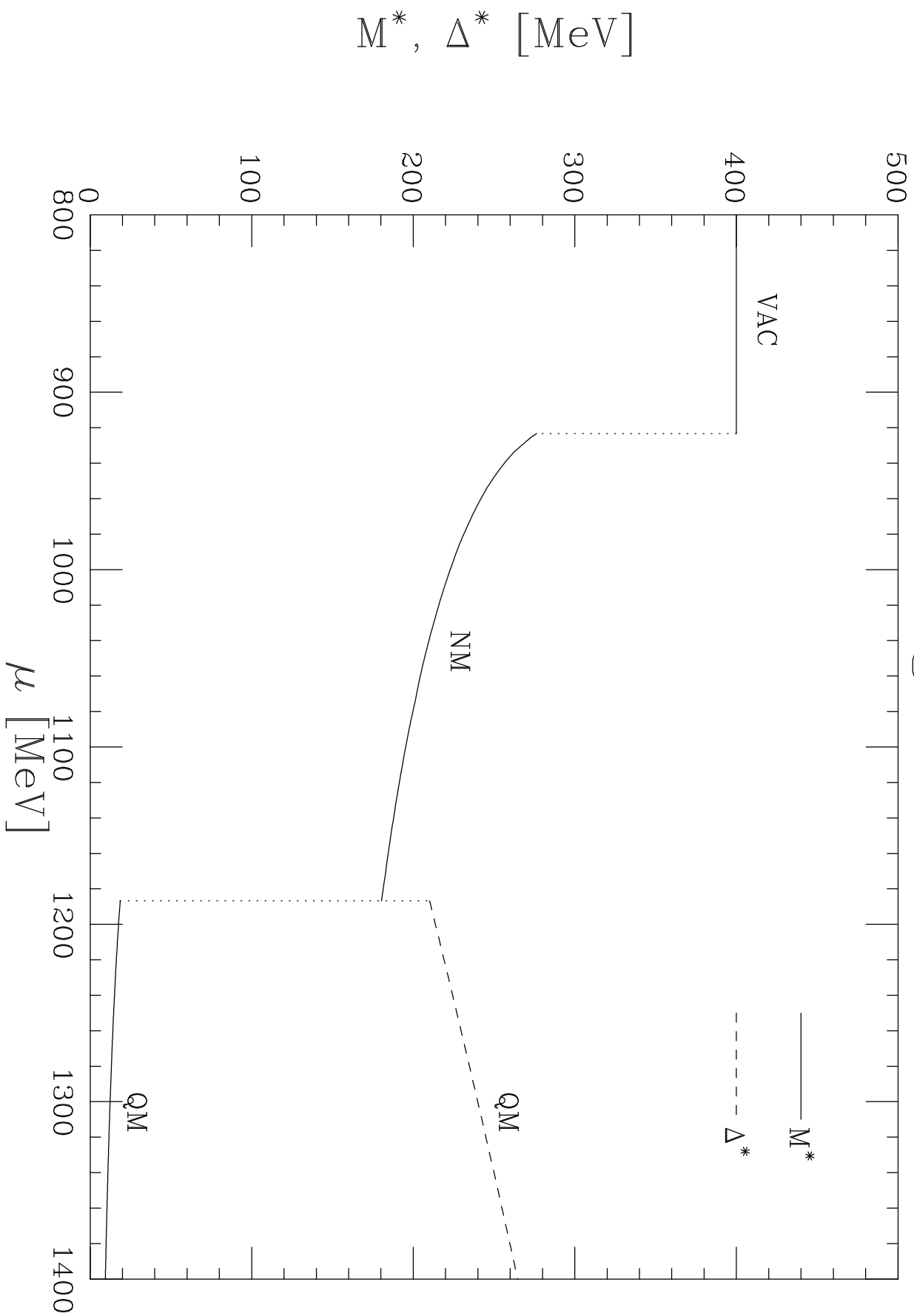


Figure 13

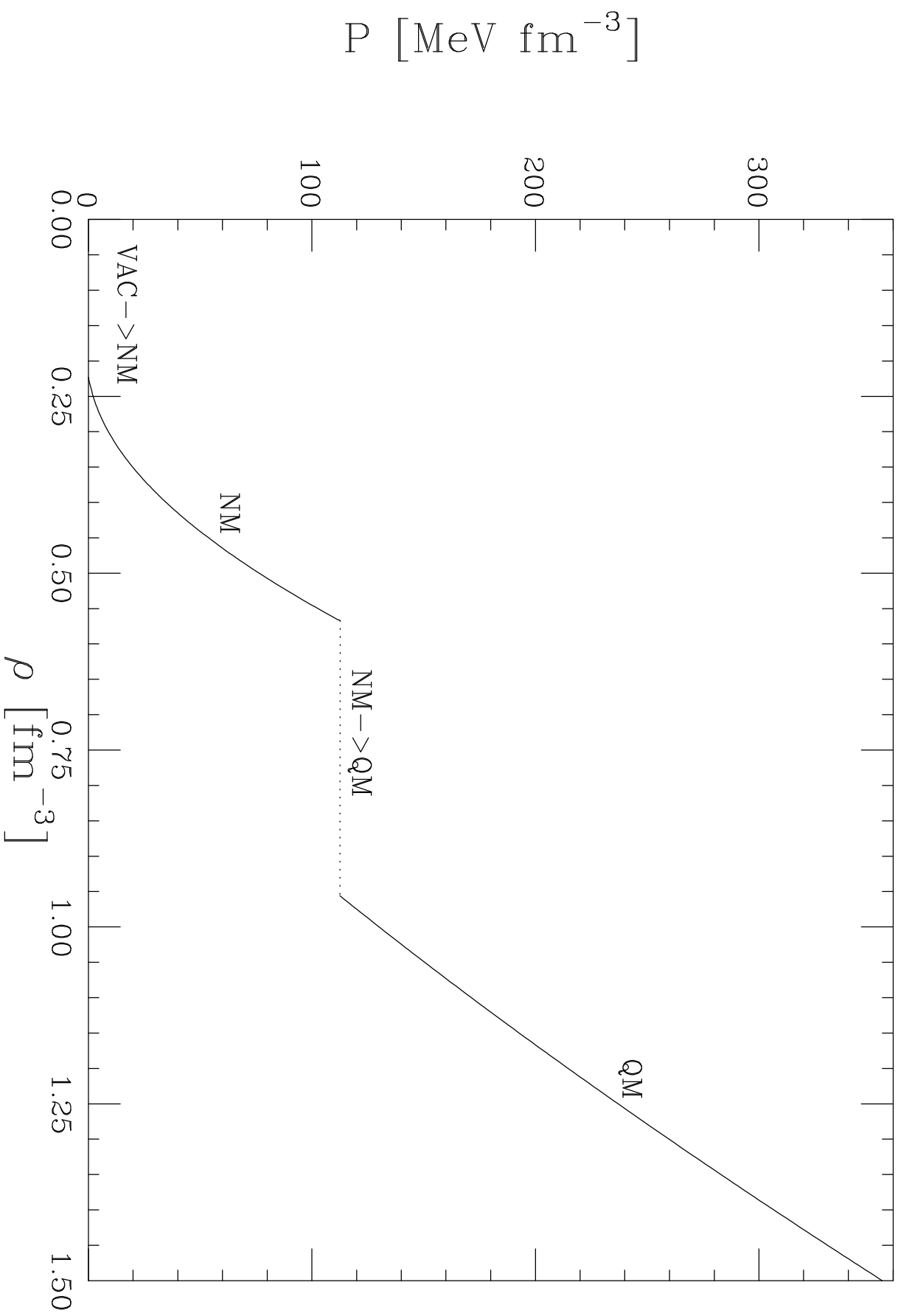


Figure 14

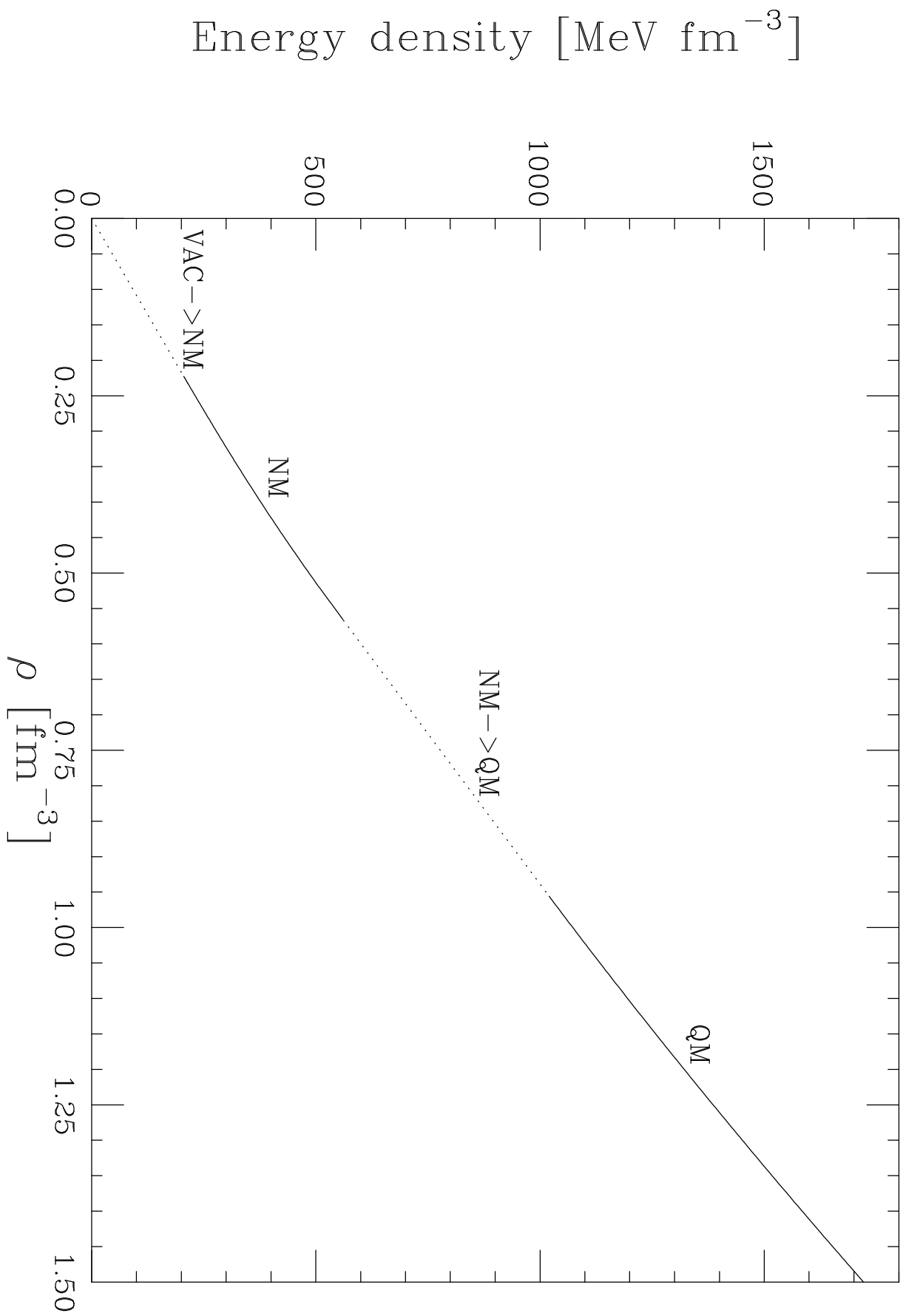


Figure 15

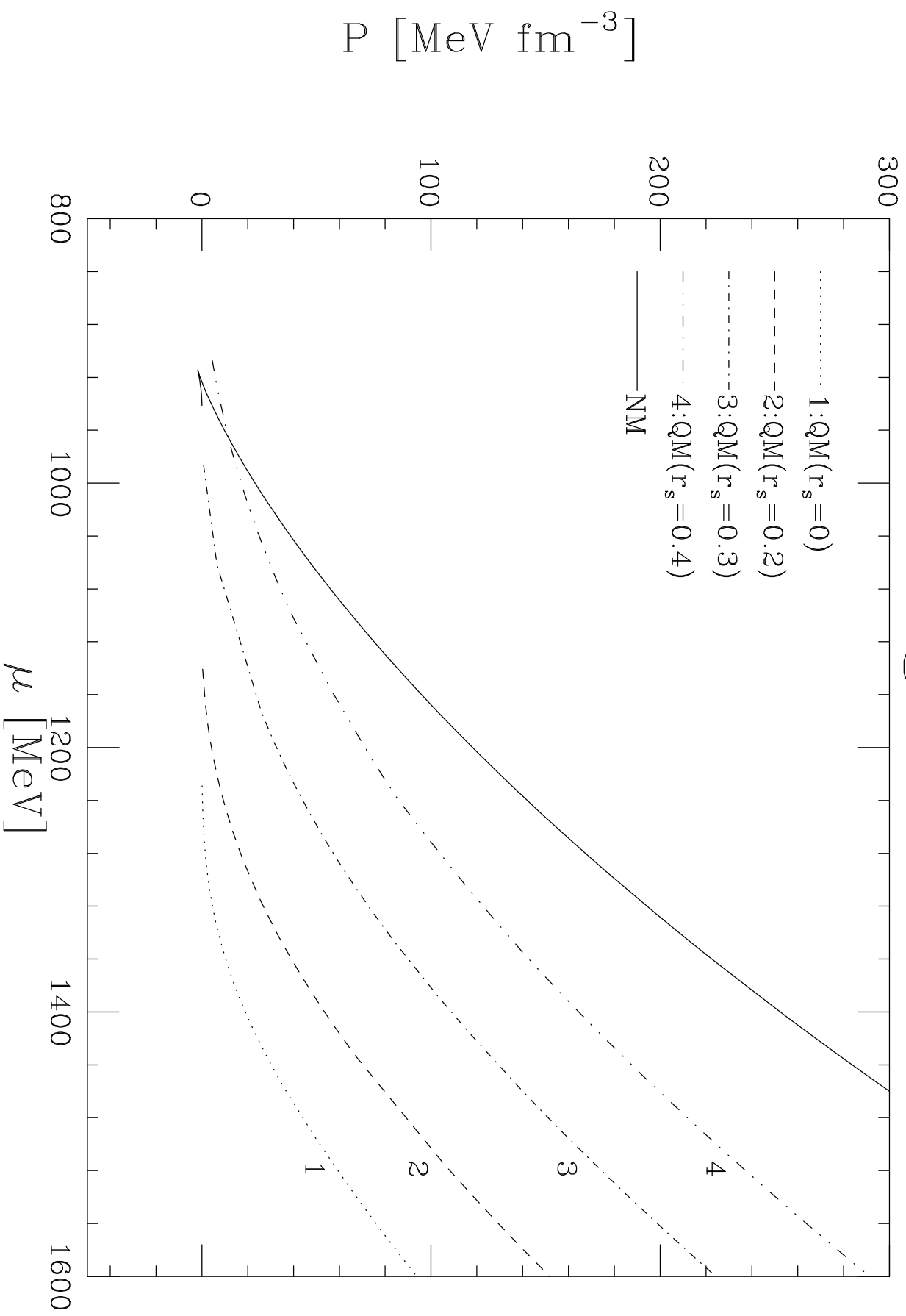


Figure 16

